Theor Chem Acc (2011) 130:645–669
DOI 10.1007/s00214-011-0985-x

REGULAR ARTICLE

An application of double exponential formula to radial quadrature grid in density functional calculation

Masaki Mitani

Received: 2 January 2011 / Accepted: 24 June 2011 / Published online: 14 July 2011

Abstract We report an application of the double exponential formula to the numerical integration of the radial electron distribution function for atomic and diatomic molecular systems with a quadrature grid. Three types of mapping transformation in the double exponential formula are introduced into the radial quadrature scheme to generate new radial grids. The double exponential grids are examined for the electron-counting integrals of He, Ne, Ar, and Kr atoms which include occupied orbitals up to the 4p shell. The performance of radial grid is compared for the double exponential formula and the formulas proposed in earlier studies. We mainly focus our attention on the behavior of accuracy by the quadrature estimation for each radial grid with varying the mapping parameter and the number of grid points. The convergence behavior of the radial grids with high accuracy for atomic system are also examined for the electron-counting integrals of LiH, NaH, KH, Li_2, Na_2, K_2, HF, HCl, HBr, F_2, Cl_2, Br_2, LiF, NaCl, KBr, $[ScH]^+$, $[MnH]^+$, and $[CuH]^+$ molecules. The results reveal that fast convergence of the integrated values to the exact value is achieved by applying the double exponential formula. It is demonstrated that the double exponential grids show similar or higher accuracies than the other grids particularly for the Kr atom, Br_2 molecule, alkali metal hydrides, alkali metal halogenides, and transition metal hydride cations, suggesting that the double exponential transformations have potential ability to improve the reliability and efficiency of the numerical integration for energy functionals.

Keywords Double exponential formula · Numerical integration · Radial quadrature grid · Electron-counting integral · Density functional calculation

1 Introduction

Density functional theory (DFT) represents the energy components of a molecule as the functional of the electron density and its derivatives. In the Kohn–Sham approximation, the exchange and correlation energies are calculated by numerical integration of the approximated functional for the exchange and correlation terms, respectively. Since the numerical integration is performed with a quadrature grid over a molecule, the accuracy depends on the number and distribution of the grid points. As the number of grid points goes to infinity, the numerical integration approaches the exact solution. However, it is desired to develop an integration scheme that gives accurate results with a small number of grid points for an application of the DFT method to large-scale and/or long-time computations such as dynamics simulation of biomolecules or materials.

A fuzzy cell method has been proposed to decompose the multi-center integral for a molecule into the single-center integrals for each atom [1]. The integrand of molecular integral is partitioned to the atomic components.

Dedicated to Professor Akira Imamura on the occasion of his 77th birthday and published as part of the Imamura Festschrift Issue.

Electronic supplementary material The online version of this article (doi:10.1007/s00214-011-0985-x) contains supplementary material, which is available to authorized users.

M. Mitani (✉)
Department of Chemistry for Materials,
Graduate School of Engineering, Mie University,
1577 Kurima-machiya, Tsu, Mie 514-8507, Japan
e-mail: mitani@chem.mie-u.ac.jp

$$I = \int F(\vec{r})\mathrm{d}^3\vec{r} \tag{1}$$

$$F(\vec{r}) = \sum_A F_A(\vec{r}) \tag{2}$$

$$F_A(\vec{r}) = w_A(\vec{r})F(\vec{r}) \tag{3}$$

$$\sum_A w_A(\vec{r}) = 1 \tag{4}$$

$F(\vec{r})$ and $F_A(\vec{r})$ are an arbitrary multi-center function and its single-center component associated with atom A, respectively. $w_A(\vec{r})$ describes the nuclear weight function for atom A to divide the whole system into the fuzzy cells. The multi-center integral of Eq. 1 can reduce to a sum of the single-center integrals.

$$I = \sum_A \int F_A(\vec{r})\mathrm{d}^3\vec{r} = \sum_A I_A \tag{5}$$

The single-center integral of Eq. 5 is evaluated in the spherical polar coordinate system centered on the nucleus of atom A as follows.

$$I_A = \int_0^\infty \int_0^\pi \int_0^{2\pi} F_A(r_A, \theta_A, \phi_A) r_A^2 \mathrm{d}r_A \sin\theta_A \mathrm{d}\theta_A \mathrm{d}\phi_A \tag{6}$$

The three-dimensional integral of Eq. 6 is approximated by successive numerical integration for the two-dimensional angular and one-dimensional radial parts using the n-point quadrature formula with the weights w^Ω and w^r as given in Eqs. 7 and 8.

$$\begin{aligned}\bar{F}_A(r_A) &= \int_0^\pi \int_0^{2\pi} F_A(r_A, \theta_A, \phi_A) \sin\theta_A \mathrm{d}\theta_A \mathrm{d}\phi_A \\ &\approx \sum_{j=1}^{n_A^\Omega} w_j^\Omega F_A\left(r_A, \Omega_j\right)\end{aligned} \tag{7}$$

$$I_A = \int_0^\infty \bar{F}_A(r_A) r_A^2 \mathrm{d}r_A \approx \sum_{i=1}^{n_A^r} w_i^r \bar{F}_A(r_i) \tag{8}$$

Ω indicates a combined spherical variable of (θ, ϕ). n_A^Ω and n_A^r are the number of grid points in the angular and radial integration for atom A, respectively.

It is possible to efficiently integrate the angular part given in Eq. 7 by using the angular grids developed by Lebedev [2]. The Lebedev grids with various number of the quadrature points on the surface of a unit sphere have been constructed so as to be invariant under the octahedron group with inversion. The smallest grid is the 6-point grid, and the largest grid is the 5810-point grid [2–7]. Each of the Lebedev grids can accurately integrate all the spherical harmonics and all the squares of spherical harmonics, respectively, up to a given maximum angular momentum of $l_{\max}$ and $l_{\max 2}$ such as $l_{\max} = 5$ and $l_{\max 2} = 2$ for the 14-point grid, $l_{\max} = 11$ and $l_{\max 2} = 5$ for the 110-point grid, $l_{\max} = 21$ and $l_{\max 2} = 10$ for the 170-point grid, $l_{\max} = 31$ and $l_{\max 2} = 15$ for the 350-point grid, $l_{\max} = 41$ and $l_{\max 2} = 20$ for the 590-point grid, and $l_{\max} = 53$ and $l_{\max 2} = 26$ for the 974-point grid. Lebedev grids are frequently available in quantum chemistry programs, for example, Gaussian, NWChem, Q-Chem, Gamess, and so on.

On the other hand, many different schemes have been introduced into the problems related to the radial integration given in Eq. 8 [1, 8–19]. The earlier representative radial grids are based on the standard method of the Gauss–Chebyshev formula or the Euler–Maclaurin formula [1, 8–10]. Recently, a multi-exponential grid [11] and a basis set adaptive grid [12] have been developed for the purpose of the efficient evaluation of radial integrals. The recent radial grids also apply the Gaussian quadrature formula to the calculation of numerical integrals. The performance for some of these radial grids has been compared with each other [10, 11, 13, 17, 19, 20].

To reduce sampling points required in numerical integration, a grid pruning technique has been considered [8–10, 20–22]. The pruning procedure is performed by assigning a different angular grid to each of radial points instead of applying common angular grid to all the radial points. The electron density distribution in a molecule becomes almost spherically symmetrical at radial points close to the nucleus of a given atom. Consequently, it is possible to use angular grids of small size for the core region in such a way that loss of accuracy is acceptably small. The most of standard fixed grids employed in popular DFT codes are pruned for efficiency.

The sensitivity of molecular properties obtained by DFT calculations to the integration grid meshes has been investigated by the program packages of Gaussian, Molpro, NWChem, Q-Chem, and Gamess [23–25]. The energetics, geometries, vibrational frequencies, and infrared intensities were examined for CCH radial, $TaCl_2$, Ge_2H_5, Ge_2H_6, $HIr[PR_3]_4Cl^+$ (R = H, CH_3) [23]. It was reported that problems with typical production grid sizes are particularly acute for third-row transition metal systems, but may still result in qualitatively incorrect results for a molecule as simple as CCH. The use of pruned coarse grids for the coupled perturbed Kohn–Sham equation caused spurious negative eigenvalues in the Hessian matrix or artificial loss of vibrational mode degeneracy. Sufficiently fine-meshed grids for typical first- and second-row systems were no longer adequate for systems involving very heavy elements such as third-row transition metals [23]. The intermonomer separations, binding energies, and potential energy surfaces were studied for dispersion-bound dimers of Ne_2, Ar_2,

$(CH_4)_2$, $(C_2H_4)_2$, and $(C_6H_6)_2$ using twenty-five density functionals [24]. It was found that VSXC, B1B95, BB95, BB1K, OLYP, and O3LYP predict oscillations and multiple minima in the potential energy surfaces of some dimers when standard grids are used. Increasing the integration grid size resulted in smoother but not necessarily single-minimum potential energy surfaces. This problem was common to the meta-generalized gradient approximation (meta-GGA) [24]. Energetic behavior for the G2/97 subset including ninety-three neutral molecules was determined to provide guidelines concerning the precision to be expected for various integration grid quadratures [25]. The errors of alcohols and thioalcohols did not go down nearly as far as the full set for the BLYP computations with a large grid, suggesting that few of these molecules could be computed precisely. For the non-Abelian subset, pathological cases with poor precision increased when higher precision was sought through use of a larger grid quadrature [25]. While the use of a much larger grid will avoid the problems mentioned above, the computation time may be unacceptably long. Therefore, it is needed to design an integration grid for both of radial and angular parts that give a result of the highest precision with the minimum number of sampling points.

The use of double exponential (DE) formula as an efficient numerical integration scheme has been proposed by Takahashi and Mori [26]. The quadrature grid of the DE formula is derived from a variable transformation followed by an application of the trapezoidal rule with an equal mesh size between grid points. The DE integration scheme is characterized by the integral being transformed over arbitrary intervals into an infinite integral in which the transformed integrand double exponentially decays near the end points of the transformed interval of integration. A family of the transformations has been given according to the type of integral [26–30].

The purpose of this paper is to demonstrate the characteristic features of the DE formula in the application to numerical integration of the radial electron distribution function for atomic and diatomic molecular systems. It has been reported that the error in the integration of electron density is a reliable guide to the error expected for the exchange and correlation energies [8, 9]. The accuracy and convergence of the DE grids are compared with those of the previous grids on the electron-counting integral of noble gas atoms using the Gauss-type orbital (GTO) and Slater-type orbital (STO) basis functions and diatomic molecules composed of hydrogen, alkali metal, transition metal, and halogen using the GTO basis functions.

2 Radial grids in earlier studies

In this section, we briefly summarize the radial grids proposed in earlier studies [1, 8–12]. The radial grid to evaluate the radial integral given in Eq. 8 is generated by combining a quadrature rule with a variable transformation. The transformation is necessary to map the variable of the quadrature grid x on the variable of the radial grid r.

$$r = \alpha t(x) \tag{9}$$

The mapping transformation includes an adjustable parameter α which varies the distribution of sampling points in the radial grid. The accuracy of numerical integration, thus, depends on the mapping parameter α for each atomic species. The Gauss–Chebyshev integration rule of the second kind and the Euler–Maclaurin summation formula (actually, the extended trapezoidal rule), respectively, given by Eqs. 10 and 11 have been used frequently as the n-point quadrature rule in the previous studies [1, 8–10, 13, 14, 18, 20].

$$\int_{-1}^{1} \left(1-x^2\right)^{1/2} F(x)\mathrm{d}x \approx \frac{\pi}{n+1}\sum_{i=1}^{n} \sin^2\left(\frac{i\pi}{n+1}\right) F(x_i)$$
$$\text{with } x_i = \cos\left(\frac{i\pi}{n+1}\right) \tag{10}$$

$$\int_{0}^{1} F(x)\mathrm{d}x \approx \frac{1}{n+1}\sum_{i=1}^{n} F(x_i) \text{ with } x_i = \frac{i}{n+1} \tag{11}$$

Becke combined the transformation of Eq. 12 and the quadrature rule of Eq. 10 [1]. The combination leads to the radial grid given in Eq. 13 (B grid).

$$t(x) = \frac{1+x}{1-x} \tag{12}$$

$$\int_{0}^{\infty} f(r)r^2\mathrm{d}r \approx 2\alpha^3 \frac{\pi}{n+1}\sum_{i=1}^{n} \frac{(1+x_i)^{5/2}}{(1-x_i)^{7/2}} f(r_i)$$
$$\begin{cases} r_i = \alpha\dfrac{1+x_i}{1-x_i} \\ w_i = 2\alpha^3 \dfrac{\pi}{n+1}\dfrac{(1+x_i)^{5/2}}{(1-x_i)^{7/2}} \end{cases} \tag{13}$$

The mapping parameter α was chosen to be half of the Bragg-Slater radius, except for H atom for which the full Bragg-Slater radius was applied.

Murray, Handy, and Laming investigated the transformation of Eq. 14 using the quadrature rule of Eq. 11 [8]. It was reported that the best results are obtained with $\beta = 2$. The radial grid for $\beta = 2$ is given in Eq. 15 (MHL grid).

$$t(x) = \frac{x^{\beta}}{(1-x)^{\beta}} \tag{14}$$

$$\int_0^{\infty} f(r) r^2 \mathrm{d}r \approx 2\alpha^3 \frac{1}{n+1} \sum_{i=1}^{n} \frac{x_i^5}{(1-x_i)^7} f(r_i)$$

$$\begin{cases} r_i = \alpha \dfrac{x_i^2}{(1-x_i)^2} \\ w_i = 2\alpha^3 \dfrac{1}{n+1} \dfrac{x_i^5}{(1-x_i)^7} \end{cases} \tag{15}$$

It was found that a good value for the mapping parameter α is the Bragg-Slater radius.

Treutler and Ahlrichs tested the combinations of four-type transformations with the Gauss–Chebyshev integration rules of the first and second kinds. A third formula for the Gauss–Chebyshev integration rule which is a variant of the first kind based on a different weight function was also examined [9]. It was confirmed that the best performance is obtained by applying the combination using the transformation of Eq. 16 and the quadrature rule of Eq. 10 for $\gamma = 0.6$. The radial grid with $\gamma = 0.6$ is given in Eq. 17 (TA grid).

$$t(x) = -\frac{(1+x)^{\gamma}}{\ln 2} \ln\left(\frac{1-x}{2}\right) \tag{16}$$

$$\int_0^{\infty} f(r) r^2 \mathrm{d}r \approx \left(\frac{\alpha}{\ln 2}\right)^3 \frac{\pi}{n+1} \sum_{i=1}^{n} (1+x_i)^{1.8} \left\{ \frac{(1+x_i)^{1/2}}{(1-x_i)^{1/2}} \ln^2\left(\frac{1-x_i}{2}\right) - 0.6 \frac{(1-x_i)^{1/2}}{(1+x_i)^{1/2}} \ln^3\left(\frac{1-x_i}{2}\right) \right\} f(r_i)$$

$$\begin{cases} r_i = -\alpha \dfrac{(1+x_i)^{0.6}}{\ln 2} \ln\left(\frac{1-x_i}{2}\right) \\ w_i = \left(\frac{\alpha}{\ln 2}\right)^3 \frac{\pi}{n+1} (1+x_i)^{1.8} \left\{ \frac{(1+x_i)^{1/2}}{(1-x_i)^{1/2}} \ln^2\left(\frac{1-x_i}{2}\right) - 0.6 \frac{(1-x_i)^{1/2}}{(1+x_i)^{1/2}} \ln^3\left(\frac{1-x_i}{2}\right) \right\} \end{cases} \tag{17}$$

The optimized values of the mapping parameter α for the TA grid were reported in Ref. [9] for atoms H through to Kr.

Mura and Knowles examined the transformation of Eq. 18 combined with the quadrature rule of Eq. 11 for $\delta = 2$, 3, and 4 [10]. By comparing the results obtained from the B, MHL, and TA grids, it was concluded that the radial grid with $\delta = 3$ is the most suitable grid for the radial integration. The radial grid of $\delta = 3$ is given in Eq. 19 (MK grid).

$$t(x) = -\ln\left(1 - x^{\delta}\right) \tag{18}$$

$$\int_0^{\infty} f(r) r^2 \mathrm{d}r \approx 3\alpha^3 \frac{1}{n+1} \sum_{i=1}^{n} \frac{x_i^2 \ln^2\left(1-x_i^3\right)}{1-x_i^3} f(r_i)$$

$$\begin{cases} r_i = -\alpha \ln\left(1-x_i^3\right) \\ w_i = 3\alpha^3 \dfrac{1}{n+1} \dfrac{x_i^2 \ln^2\left(1-x_i^3\right)}{1-x_i^3} \end{cases} \tag{19}$$

The recommended values of the mapping parameter α for the MK grid were listed in Ref. [10] for atoms H through to Zn.

Gill and Chien recently proposed the n-point radial grid given in Eq. 20 (MultiExp grid) on the basis of the log-squared quadrature rule of Eq. 21 and the transformation of Eq. 22 [11].

$$\int_0^{\infty} f(r) r^2 \mathrm{d}r \approx \alpha^3 \sum_{i=1}^{n} \frac{w_i}{x_i} f(r_i)$$

$$\begin{cases} r_i = -\alpha \ln x_i \\ w_i = \alpha^3 \dfrac{a_i}{x_i} \end{cases} \tag{20}$$

$$\int_0^1 \ln^2 x \, F(x) \mathrm{d}x \approx \sum_{i=1}^{n} a_i F(x_i) \tag{21}$$

$$t(x) = -\ln x \tag{22}$$

The values of roots x_i and weights a_i associated with the polynomials $Q_n(x)$ orthogonal on the interval [0, 1] were reported up to the 20-point grid in Ref. [11]. Those values are also available up to the 50-point grid via the web site [31].

Kakhiani, Tsereteli, and Tsereteli also recently developed the basis set adaptive grid generated by an automatic quadrature routine (AQR grid) [12]. In the AQR method, the integral region in radial space r is divided into finite intervals and a semi-infinite interval as $[0, \infty) = [0, r_1] + [r_1, r_2] + \cdots + [r_{n-1}, r_n] + [r_n, \infty)$. The r_1, r_2, …, r_{n-1}, and r_n correspond to the positions of maxima and minima in the radial electron distribution represented with the contracted GTO basis functions for an atom. The standard formulas of the Gauss–Legendre quadrature and the Gauss–Laguerre quadrature are directly used to carry out the finite integrations and the semi-finite integration, respectively. The number of grid points in each interval is determined so as to provide user specified accuracy by starting the iteration process with two points and increasing the number of points by one with each subsequent iteration.

The characteristic features of roots and weights were discussed in Ref. [11] for the B, MHL, TA, MK, and MultiExp quadrature schemes. The accuracies of these radial grids were also studied in Ref. [11] for the linear combination of Gaussian functions $f(r) = \exp(-r^2)$, $\exp(-r^2) + 10\exp(-10r^2)$, and $\exp(-r^2) + 10\exp(-10r^2) + 100\exp(-100r^2)$ and for the radial electron distribution function (spherically averaged radial electron density) $f(r) = 4\pi r^2\rho(r)$ of He, Ne, and Ar atoms. The performance of the AQR grid for the same set of integrands was reported in Ref. [12] by comparison to the results of Ref. [11]. However, the analysis of Ref. [11] was carried out by using the standardized grid with a small number of grid points (25 or less) in which the value of mapping parameter α is chosen so that the middle point of radial grids is unity for each quadrature scheme. The dependence of accuracy on the mapping parameter and the convergence of integrated values to the exact value were not examined.

3 Double exponential formula and radial grids

In 1974, Takahashi and Mori introduced the double exponential (DE) formula for numerical integration [26]. The DE formula apply the uniformly divided trapezoidal rule with mesh size h to infinite integral which is obtained by suitable variable transformation of a given integrand. The transformation function is chosen so as to change the lower- and upper-limits of the interval for the original integral into the minus and plus infinities for the transformed integral.

$$\int_a^b F(y)\mathrm{d}y = \int_{-\infty}^{\infty} F(t(x))\frac{\mathrm{d}t(x)}{\mathrm{d}x}\mathrm{d}x \approx h\sum_{i=-\infty}^{\infty} t'(x_i)F(t(x_i)) \text{ with } x_i = ih \tag{25}$$

$$y = t(x) \text{ where } a = t(-\infty),\ b = t(\infty) \tag{26}$$

The DE formula adopts the mapping transformation such that the transformed integrand decays double exponentially at $x \to \pm\infty$. The infinite summation appeared in Eq. 25, therefore, can be truncated appropriately in actual calculations.

The practical transformations of DE formula were given in Refs. [26–30] for the finite, semi-infinite, and infinite integrals. Three-type transformations were proposed for the semi-infinite integral with the interval of $0 \le y \le \infty$.

$$y = \exp\left(\frac{\pi}{2}\sinh x\right) \text{ or } \exp(2\sinh x) \text{ or } \exp(\pi\sinh x) \tag{27}$$

$$y = \exp(x - \exp(-x)) \text{ or } \exp\left(\frac{1}{2}x - \exp(-x)\right) \tag{28}$$

$$y = \ln\left(\exp\left(\frac{\pi}{2}\sinh x\right) + 1\right) \tag{29}$$

In this study, we apply the transformations of Eqs. 27–29 to the radial function in the following parameter-depending forms. The radial quadrature grids using Eqs. 30, 31, and 32 are, respectively, referred to as the DE1, DE2, and DE3 grids hereafter.

$$r = \exp(\alpha\sinh x) \tag{30}$$

$$r = \exp(\alpha x - \exp(-x)) \tag{31}$$

$$r = \ln(\exp(\alpha\sinh x) + 1) \tag{32}$$

The DE grids are represented as Eqs. 33–35 for the DE1-DE3 grids, respectively.

$$\int_0^{\infty} f(r)r^2\mathrm{d}r \approx h\sum_{i=-\infty}^{\infty} \alpha\exp(3\alpha\sinh x_i)\cosh x_i f(r_i) \quad \begin{cases} r_i = \exp(\alpha\sinh x_i) \\ w_i = h\alpha\exp(3\alpha\sinh x_i)\cosh x_i \end{cases} \tag{33}$$

$$\int_0^{\infty} f(r)r^2\mathrm{d}r \approx h\sum_{i=-\infty}^{\infty} \exp(3\alpha x_i - 3\exp(-x_i)) \times(\alpha + \exp(-x_i))f(r_i) \quad \begin{cases} r_i = \exp(\alpha x_i - \exp(-x_i)) \\ w_i = h\exp(3\alpha x_i - 3\exp(-x_i))(\alpha + \exp(-x_i)) \end{cases} \tag{34}$$

$$\int_0^{\infty} f(r)r^2\mathrm{d}r \approx h\sum_{i=-\infty}^{\infty} \ln^2(\exp(\alpha\sinh x_i) + 1) \times\frac{\exp(\alpha\sinh x_i)\alpha\cosh x_i}{\exp(\alpha\sinh x_i) + 1}f(r_i) \quad \begin{cases} r_i = \ln\{\exp(\alpha\sinh x_i) + 1\} \\ w_i = h\ln^2(\exp(\alpha\sinh x_i) + 1)\dfrac{\exp(\alpha\sinh x_i)\alpha\cosh x_i}{\exp(\alpha\sinh x_i) + 1} \end{cases} \tag{35}$$

4 Computational details

In this study, the electron-counting integrals for He, Ne, and Ar atoms were examined to compare the performance of the DE grids with the performance of the B, MHL, TA, MK, MultiExp, and AQR grids reported in Refs. [11] and [12]. We also examined the electron-counting integral for Kr atom to investigate the applicability of various radial grids to heavy elements including occupied 3d shells. The radial electron distribution of the atoms at the Hartree–Fock level was calculated with the contracted GTO basis functions of the 6-311G basis set [32–34] as used in Refs. [11] and [12]. The SCF atomic orbitals were obtained from the formatted checkpoint file of Gaussian03 program [35].

Table 1 Optimized interatomic distance of LiH, NaH, KH, Li_2, Na_2, K_2, HF, HCl, HBr, F_2, Cl_2, Br_2, LiF, NaCl, KBr, $[ScH]^+$, $[MnH]^+$, and $[CuH]^+$ molecules at B3LYP level

Molecule	Distance (Å)	Molecule	Distance (Å)	Molecule	Distance (Å)
LiH	1.615	NaH	1.882	KH	2.284
Li_2	2.727	Na_2	3.040	K_2	3.966
HF	0.925	HCl	1.286	HBr	1.423
F_2	1.406	Cl_2	2.044	Br_2	2.335
LiF	1.552	NaCl	2.376	KBr	2.872
$[ScH]^+$ ($^2\Delta$)	1.756	$[MnH]^+$ ($^6\Sigma$)	1.598	$[CuH]^+$ ($^2\Sigma$)	1.506

We also calculated the radial electron distribution of the atoms at the Hartree–Fock level using the primitive STO basis functions reported in Ref. [36] as 4s for He atom, 7s5p for Ne atom, 10s8p for Ar atom, and 11s10p5d for Kr atom. The SCF atomic orbitals were taken from Ref. [36].

The infinite summation of DE formula indicated in Eqs. 33–35 was approximated by the finite sum of the quadrature points corresponding to the radial points distributed from $r = 10^{-7}$ to $r = 10R$ (GTO) or $20R$ (STO), where R denotes the atomic radius. We used the expectation value of orbital radius for the outer valence orbital of the atoms as the values of R: $R_{He} = 0.927272$ Bohr, $R_{Ne} = 0.965273$ Bohr, $R_{Ar} = 1.662954$ Bohr, and $R_{Kr} = 1.951590$ Bohr, which were obtained by the Hartree–Fock calculations with the primitive STO basis functions [36].

Furthermore, in addition to the atomic integrals described above, the electron-counting integrals for LiH, NaH, KH, Li_2, Na_2, K_2, HF, HCl, HBr, F_2, Cl_2, Br_2, LiF, NaCl, KBr, $[ScH]^+$, $[MnH]^+$, and $[CuH]^+$ molecules were examined by the TA, MK, and DE radial grids as test cases for molecular integrals. A fairly large Lebedev angular grid of 1202 grid points was combined with the radial grid to clarify the performance of radial grid by minimizing the error of angular grid. The electron density of the molecules was computed at the DFT level approximated with the B3LYP exchange and correlation functional [37, 38] in the restricted (MH, M_2, HX, X_2, and MX with M = alkali metal and X = halogen) or unrestricted ($[MH]^+$ with M = transition metal) form using the contracted GTO basis functions. The 6-31G** basis set [39–46] and the VDZ basis set [47] were employed as the basis functions for H, Li, Na, K, F, Cl, and Br atoms and for Sc, Mn, and Cu atoms, respectively. The SCF molecular orbitals were extracted from the formatted checkpoint file of Gaussian03 program [35]. The interatomic distances of the diatomic molecules were optimized as shown in Table 1 by the restricted and unrestricted B3LYP methods for closed-shell (MH, M_2, HX, X_2, and MX) and open-shell ($[MH]^+$) molecules, respectively. All the stationary points were confirmed to be energy minima with real vibrational frequencies. The geometry optimization and the frequency analysis were carried out by Gaussian03 program [35].

The infinite summation of quadrature estimation appeared in Eqs. 33–35 for the DE formula was started at the radial point of $r = 10^{-7}$ and truncated at the radial point of $r = 10R$ (M in MH, M_2, HX, X_2, M in MX, and M in $[MH]^+$) or $20R$ (H in MH, X in MX, and H in $[MH]^+$). The following orbital radius [36] was applied to the values of atomic radius R as $R_H = 1.5$ Bohr, $R_{Li} = 3.873661$ Bohr, $R_{Na} = 4.208762$ Bohr, $R_K = 5.243652$ Bohr, $R_F = 1.084786$ Bohr, $R_{Cl} = 1.842024$ Bohr, $R_{Br} = 2.111601$ Bohr, $R_{Sc} = 3.959716$ Bohr, $R_{Mn} = 3.381917$ Bohr, and $R_{Cu} = 3.330979$ Bohr.

The exact value of the electron-counting integral gives the number of electrons for a given atom or molecule. Each of the occupied orbitals for the atoms and molecules examined in this study was renormalized to ensure that the exact numerical integration gives the exact electron number. The accuracy of numerical integration was measured by the following index introduced in Ref. [11] and also used in Ref. [12].

$$\text{Accuracy} = -\log_{10}\left|\frac{\text{Approx}}{\text{Exact}} - 1\right| \tag{36}$$

Accuracy is the quality of a quadrature approximation (Approx) of an integral in comparison with the exact value (Exact) which essentially gives the number of correct digits in the quadrature estimation. The upper limit of Accuracy is 15.7 obtained from logarithm of the machine epsilon in double precision of Fortran 90.

For atomic integrals, the changes in Accuracy with the variation of the mapping parameter α and the number of grid points n^r were investigated for the B, MHL, TA, MK, MultiExp grids as well as for the DE1, DE2, and DE3 grids. The value of α was varied by 0.1 from α_{min} to α_{max} for each radial grid: $\alpha_{min} = 0.1$ and $\alpha_{max} = 5.1$ for the B and MHL grids, $\alpha_{min} = 0.5$ and $\alpha_{max} = 5.5$ for the TA, MultiExp, and DE grids, and $\alpha_{min} = 2.5$ and $\alpha_{max} = 7.5$ for the MK grid. As for molecular integrals, the convergence behavior of Accuracy was confirmed for the TA, MK, DE1, DE2, and DE3 grids with the fixed value of α listed in Table 2 for each atom. The recommended value of α reported in Refs. [9] and [10] was used for the TA and MK grids, respectively. Concerning the MK grid, we adopted $\alpha = 5.0$ for Br atom since $\alpha = 7.0$ and $\alpha = 5.0$ have been applied to elements of the groups I (except for H atom) and II and to the other elements, respectively, for atoms H through to Zn [10]. The same value of α was

Table 2 Value of mapping parameter α for the TA, MK, DE1, DE2, and DE3 grids used to evaluate the electron-counting integrals of LiH, NaH, KH, Li_2, Na_2, K_2, HF, HCl, HBr, F_2, Cl_2, Br_2, LiF, NaCl, KBr, $[ScH]^+$, $[MnH]^+$, and $[CuH]^+$ molecules

Atom	TA[a]	MK[b]	DE1	DE2	DE3
H	0.8	5.0	1.2	1.0	2.4
Li	1.8	7.0	1.2	1.0	2.4
Na	1.4	7.0	1.2	1.0	2.4
K	1.5	7.0	1.2	1.0	2.4
F	0.9	5.0	1.2	1.0	2.4
Cl	1.0	5.0	1.2	1.0	2.4
Br	0.9	5.0	1.2	1.0	2.4
Sc	1.3	5.0	1.2	1.0	2.4
Mn	1.2	5.0	1.2	1.0	2.4
Cu	1.1	5.0	1.2	1.0	2.4

[a] Values of mapping parameter for TA grid are taken from Ref. [9]

[b] Values of mapping parameter for MK grid are taken from Ref. [10] except for Br

employed for all the atoms in the DE integration without fine tuning of the radial grid for each atom. The number of n^r was varied by 10 from $n^r = 30$ to $n^r = 200$ for all the radial grids except for the MultiExp grid which are available up to $n^r = 50$.

Becke has defined the nuclear weight function, $w_A(\vec{r})$ in Eq. 3, by introducing a cutoff profile between two nuclear centers [1]. A sequence of cutoff profiles can be determined successively by an iterative procedure as continuous analogs to the step function. It has been found that the iteration order $k = 3$ is appropriate for general applications [1]. However, it has been also reported that the convergence of integrated results to high accuracy (Accuracy > 15) is faster for $k = 4$ or 5 than for $k = 3$ in the case of H_2 molecule [16]. Therefore, we confirmed using the TA and MK quadrature schemes that $k = 5$ adopted in this study is most efficient among $k = 3$, 4, and 5 for all the diatomic molecules examined in this study. Atomic size adjustments proposed in Refs. [1] or [9] were not applied to numerical integration of the heteronuclear diatomic molecules.

5 Results and discussion

5.1 Electron-counting integral for atom

We show the changes in Accuracy of each radial grid for the numerical integration of the radial electron distribution represented with the GTO and STO basis functions in Figs. 1, 2, 3, and 4 and in Figs. 5, 6, 7, and 8, respectively, as Figs. 1 and 5 for He atom, Figs. 2 and 6 for Ne atom, Figs. 3 and 7 for Ar atom, and Figs. 4 and 8 for Kr atom. Accuracy of each radial grid with the mapping parameter which gives the highest average value of Accuracy over the 30-point to 200-point grids (over the 30-point to 50-point grids for the MultiExp grid) is also listed in Online Resources 1 and 2 as Tables S1 and S2 for the GTO and STO calculations, respectively.

All the quadrature schemes work well for all the cases of four atoms using the GTO and STO basis functions from a viewpoint that all the quadrature approximations of Figs. 1, 2, 3, 4, 5, 6, 7, and 8 converge toward the exact integration. However, different characteristic features are confirmed from Figs. 1, 2, 3, 4, 5, 6, 7, and 8 in the dependence of numerical accuracy on the mapping parameter and in the convergence of integrated values with increasing the number of grid points. The B and MHL grids have narrow sweet spot of the mapping parameter even for the large-point grids, whereas the TA, MK, and DE grids with the large number of grid points are relatively stable (flat) over the wide range of the mapping parameter. The changes in Accuracy of the B and MHL grids indicate similar behavior for the variation of mapping parameter and for the increment of grid points that the convergence to the exact result is slow in comparison with the TA, MK, and DE grids. The MultiExp grid with the optimal value of the mapping parameter results in relatively high Accuracy for the 30-point grid, but the improvement of Accuracy by applying the 40-point and 50-point grids is not remarkable especially for the STO calculations. The TA and MK grids show good performance over the 30-point to 200-point grids by selecting the value of mapping parameter appropriately in which the MK grids is better than the TA grids regarding the accuracy and the convergence as found from Tables S1 and S2 (Online Resources 1 and 2).

The grid ranking on the basis of Accuracies listed in Tables S1 and S2 (Online Resources 1 and 2) is summarized in Tables 3 (GTO) and 4 (STO) for the radial grids with $n^r = 30$, 40, and 50. The GTO results show that the DE schemes tend to be more accurate than the B or MHL scheme and less accurate than the TA or MK scheme, except for Ar ($n^r = 30$) and Kr ($n^r = 30$, 40, and 50) atoms for which the DE2 or DE3 scheme is less accurate than the B and MHL schemes. As for the STO results, the DE grids are similar to or higher than the B and MHL grids in Accuracy. Although the DE2 and DE3 grids give the highest Accuracy for He atom, the DE grids are lower than the TA or MK grid in Accuracy for Ne ($n^r = 30$), Ar ($n^r = 30$ and 40), and Kr ($n^r = 30$ and 40) atoms with sparse grids. The DE1 grid is also lower than the TA and MK grids in Accuracy for He atom with $n^r = 30$ and 40. However, the DE results converge to the exact value with Accuracy $= 15.7$ faster than the TA and MK results for

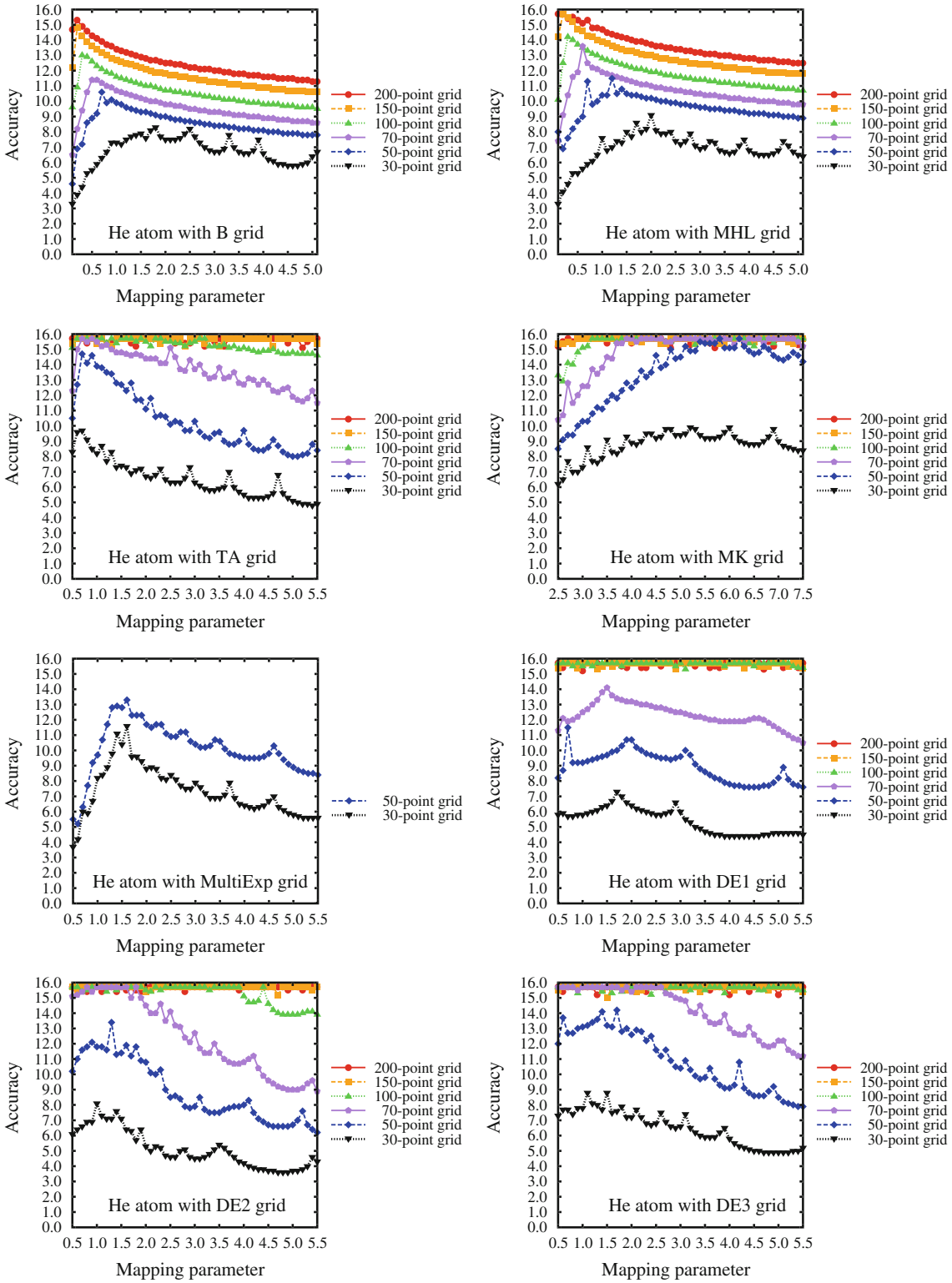

Fig. 1 Changes in Accuracy of the B, MHL, TA, MK, MultiExp, DE1, DE2, and DE3 grids for the electron-counting integral of He atom using GTO basis functions

heavy elements of the Ar and Kr atoms. The smallest number of grid points with Accuracy > 15 extracted from Tables S1 and S2 (Online Resources 1 and 2) is shown in Table 5 for the TA, MK, and DE grids. The fast convergence of the DE formula is more significant in the STO basis functions than in the GTO basis functions. Among the

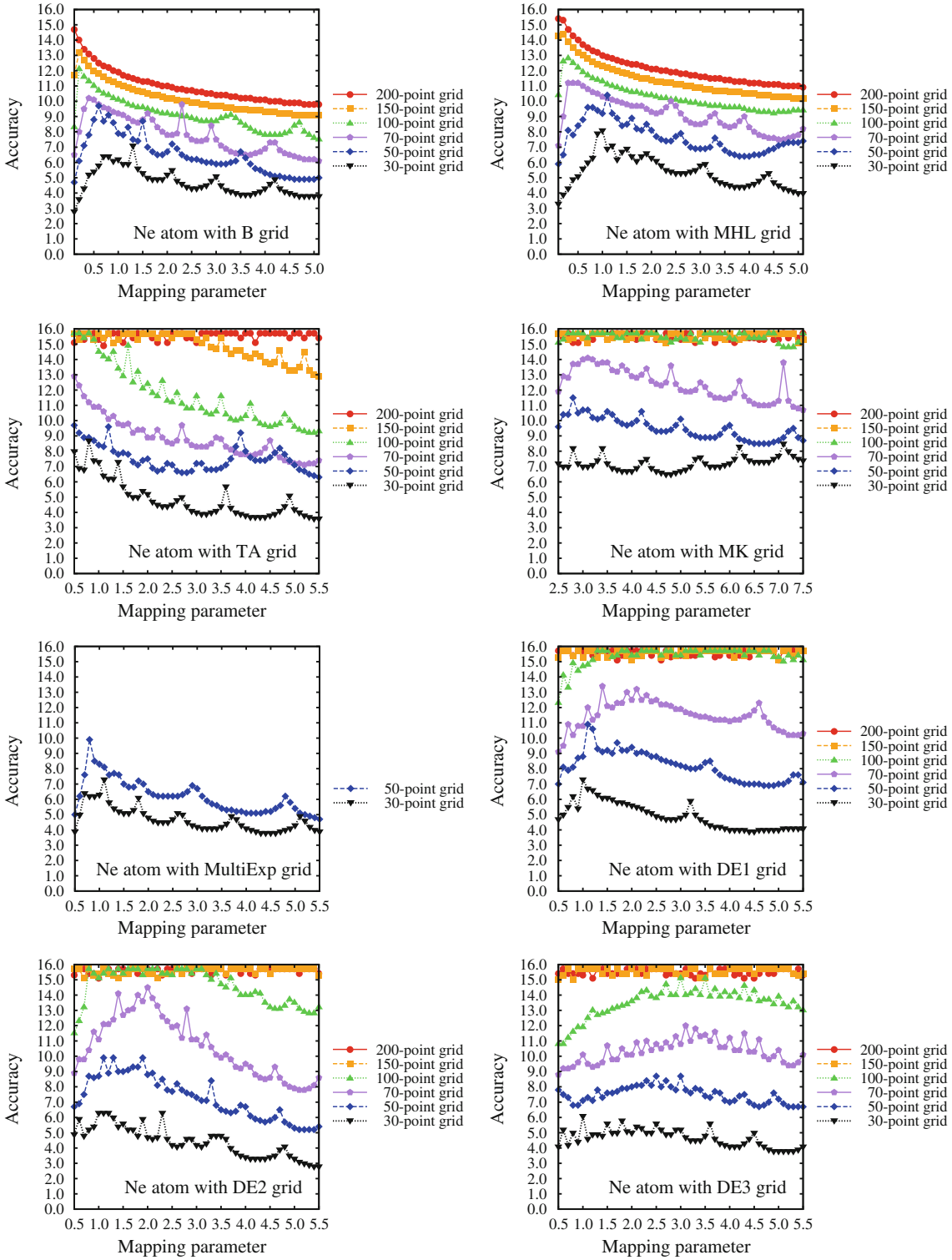

Fig. 2 Changes in Accuracy of the B, MHL, TA, MK, MultiExp, DE1, DE2, and DE3 grids for the electron-counting integral of Ne atom using GTO basis functions

DE grids, the convergence becomes slower for the DE3 grid than for the DE1 and DE2 grids in the GTO calculation and slower for the DE1 grid than for the DE2 and DE3 grids in the STO calculation.

We compare the results obtained in this study with the results reported in Refs. [11] and [12]. Accuracies of the standardized grids for the B, MHL, TA, MK, and MultiExp schemes were summarized in Ref. [11] for the electron-

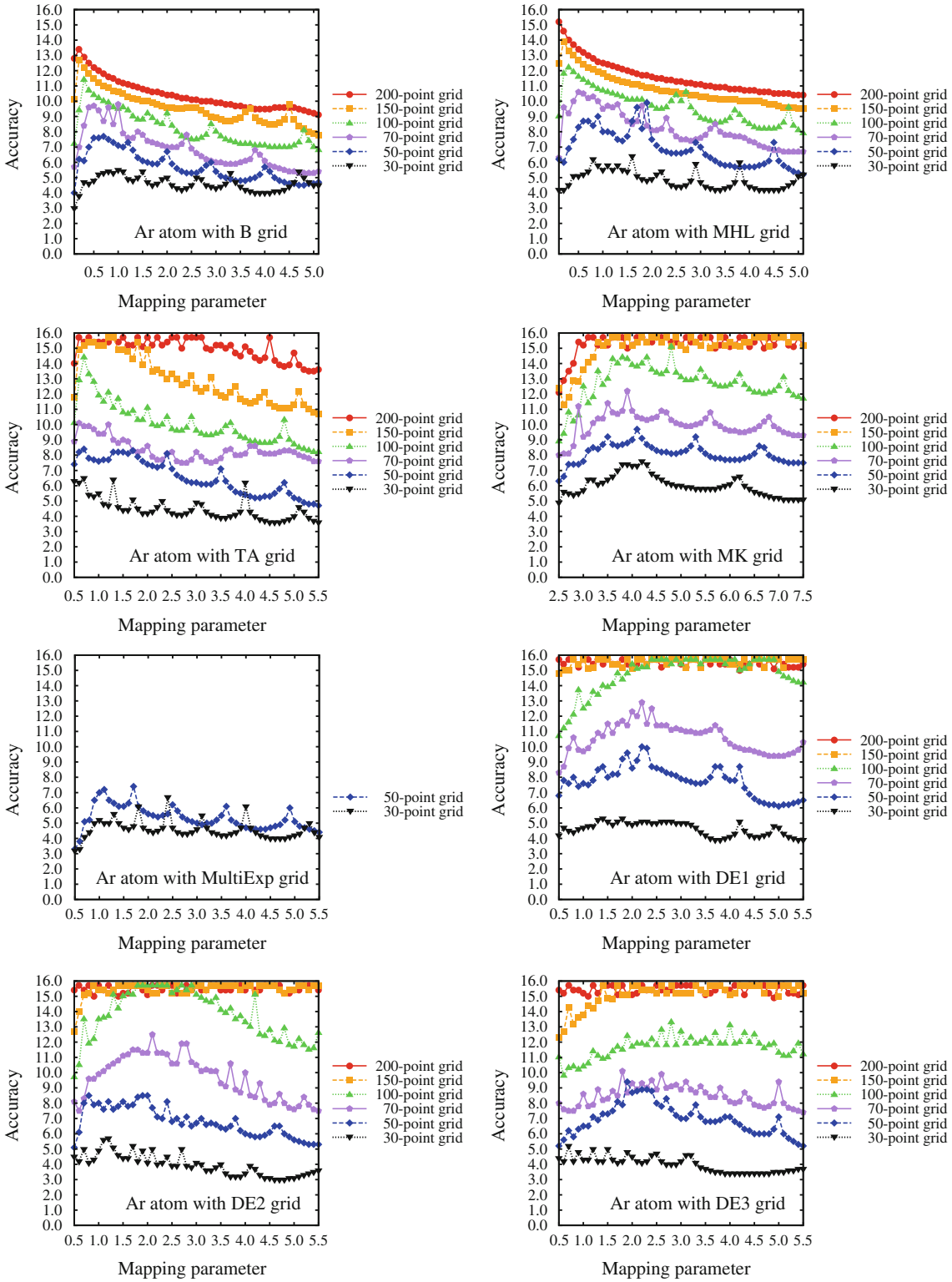

Fig. 3 Changes in Accuracy of the B, MHL, TA, MK, MultiExp, DE1, DE2, and DE3 grids for the electron-counting integral of Ar atom using GTO basis functions

counting integral of the He, Ne, and Ar atoms with the GTO basis functions. Accuracy of the AQR scheme was also listed in Ref. [12] for the same integrals. For each radial grid, the optimal value of mapping parameter is chosen based on the average Accuracy in this study while the value of mapping parameter is fixed to the standardized value in Ref. [11].

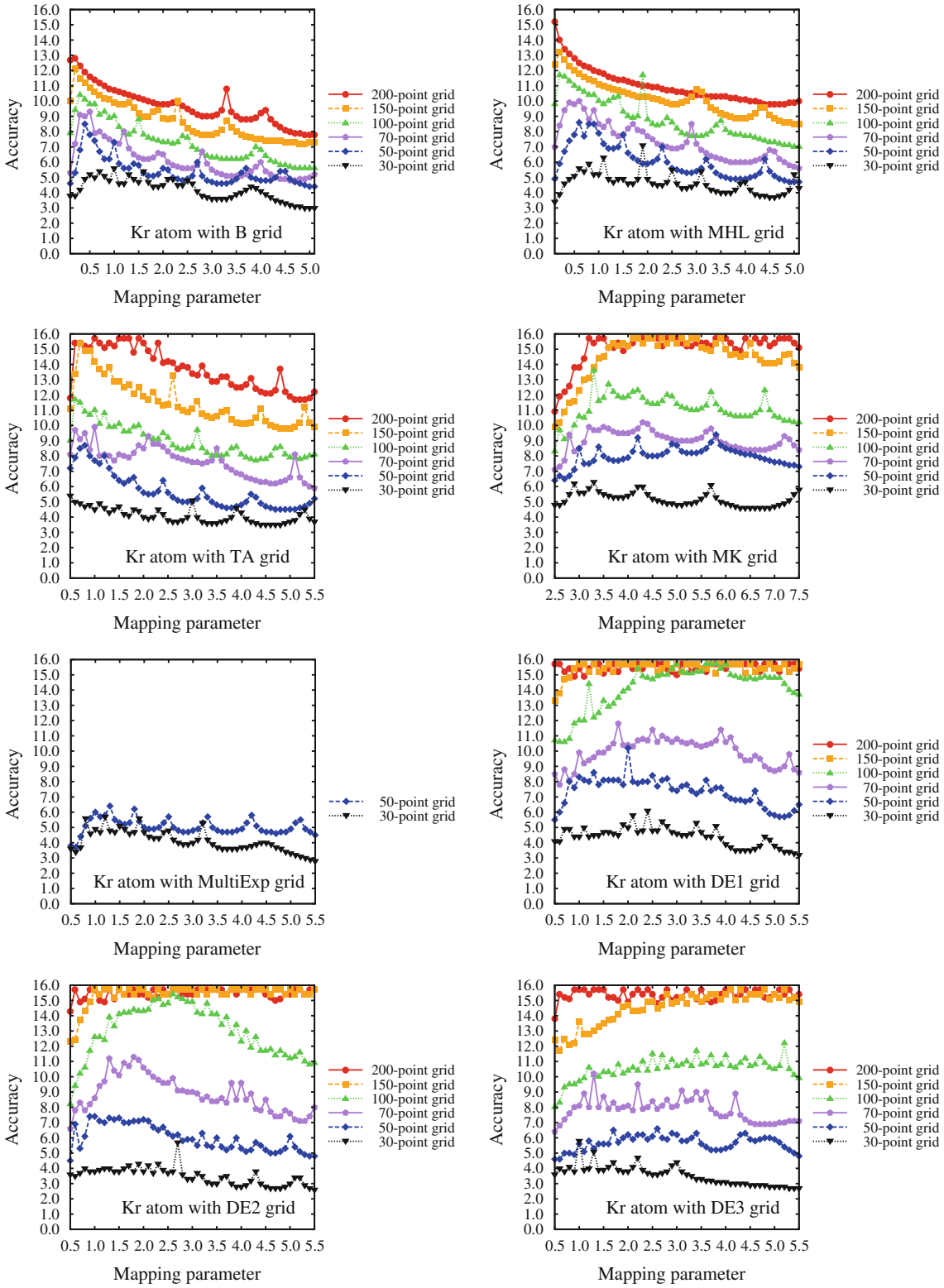

Fig. 4 Changes in Accuracy of the B, MHL, TA, MK, MultiExp, DE1, DE2, and DE3 grids for the electron-counting integral of Kr atom using GTO basis functions

The grid ranking was estimated using 25 or less grid points as follows: MHL < B < TA ≈ MK < MultiExp for He atom and MHL < TA ≈ MK < MultiExp ≈ B for Ne atom [11]. As for Ar atom, it was described that although it is no longer possible to rank the grids unambiguously, the MultiExp grid remains competitive [11]. However, by taking

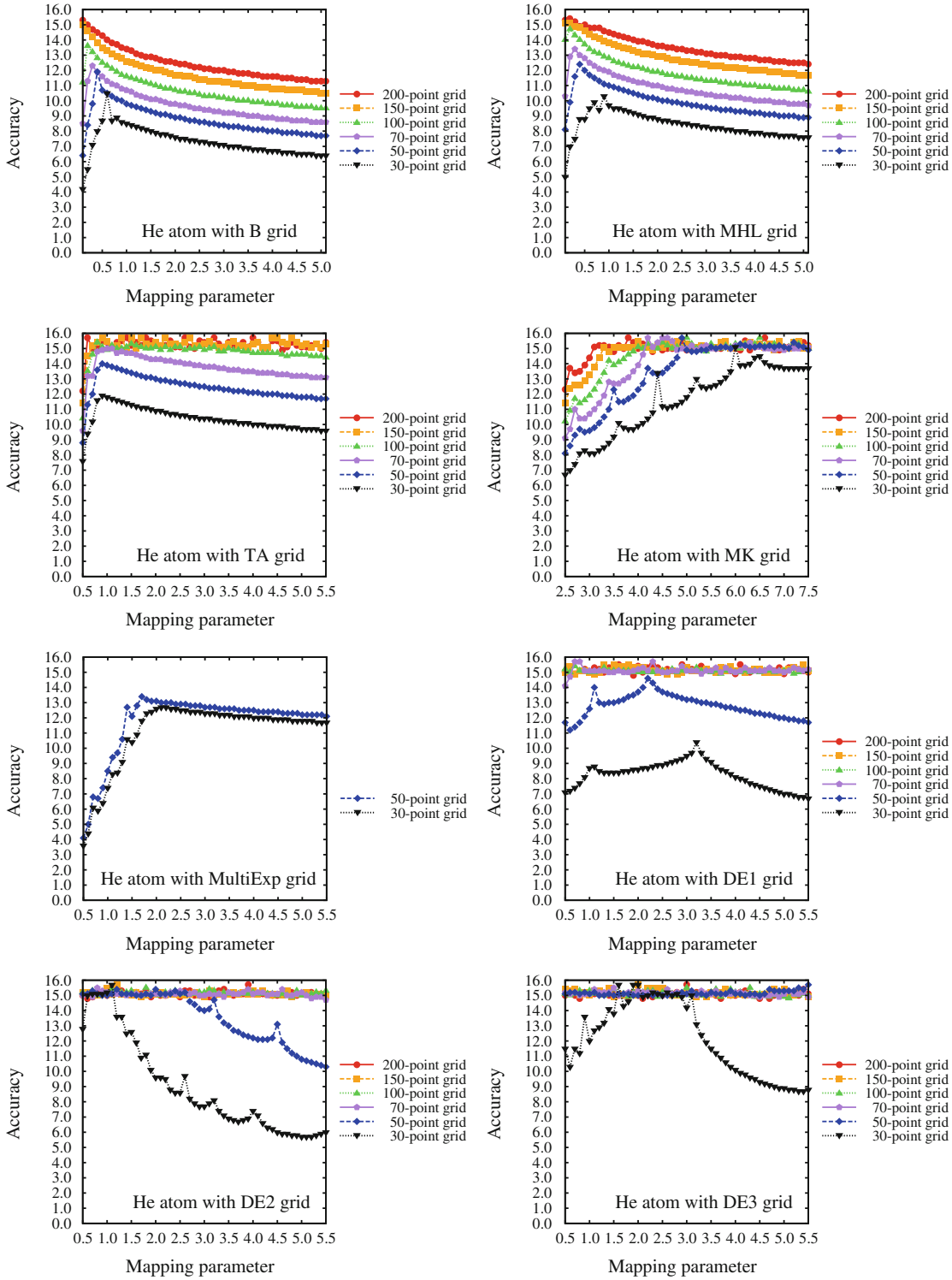

Fig. 5 Changes in Accuracy of the B, MHL, TA, MK, MultiExp, DE1, DE2, and DE3 grids for the electron-counting integral of He atom using STO basis functions

into account the optimization of the mapping parameter, Figs. 1, 2, 3, 4, 5, 6, 7, and 8 reveal that the TA and MK grids as well as the DE grids are superior to the B and MHL grids and probably to the MultiExp grid.

Accuracy of the AQR grid reported in Ref. [12] is compared with Accuracies of the TA, MK, and DE2 grids given in Table S1 (Online Resource 1). We list the results for He, Ne, and Ar atoms in Table 6. The

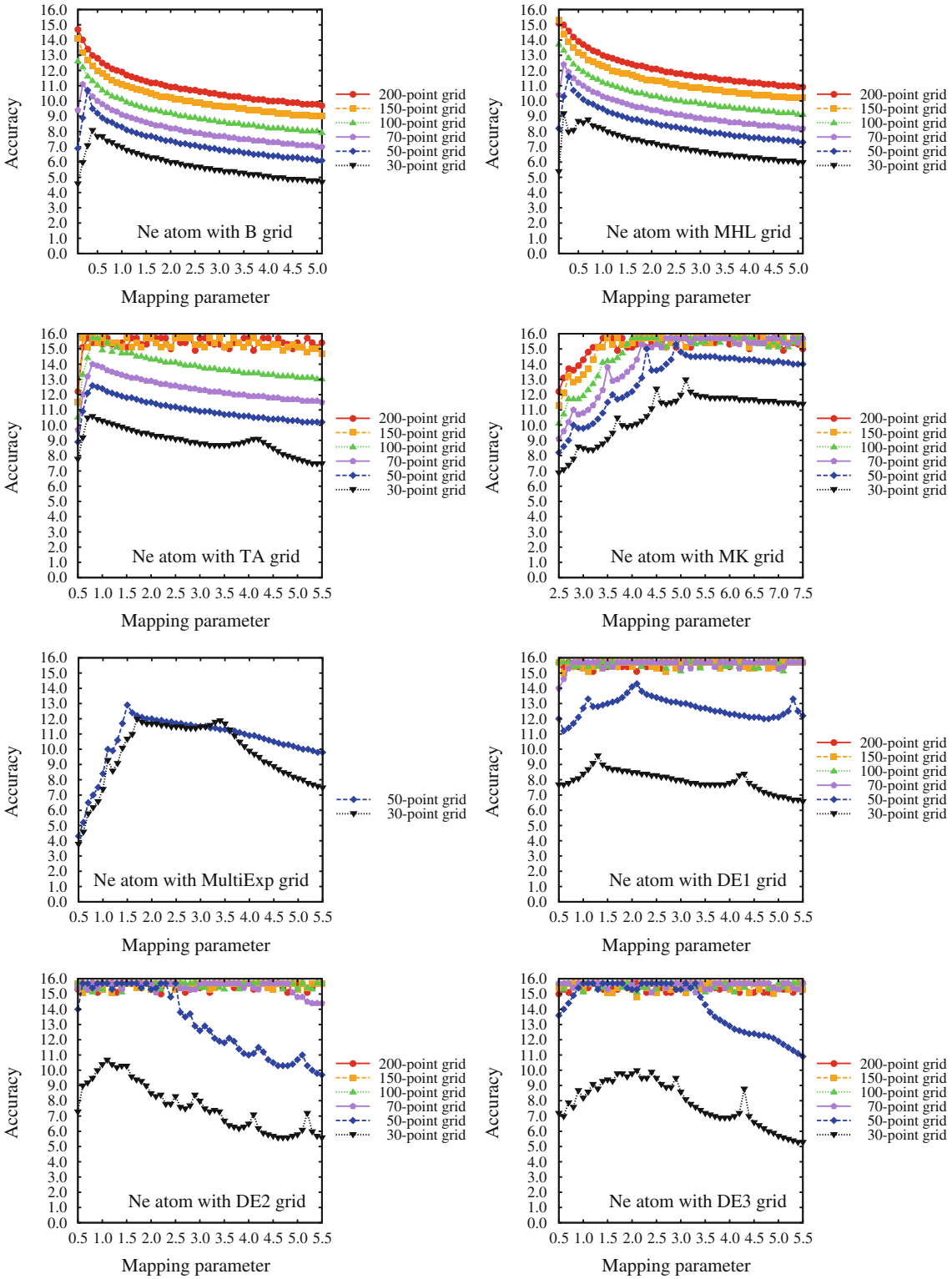

Fig. 6 Changes in Accuracy of the B, MHL, TA, MK, MultiExp, DE1, DE2, and DE3 grids for the electron-counting integral of Ne atom using STO basis functions

AQR results seem to be somewhat better than the TA and MK results for simple radial electron distribution of the He atom without shell structure. Concerning the Ne and Ar atoms with shell structure, the effectiveness of the basis set adaptive grid over the fixed grids may be unclear.

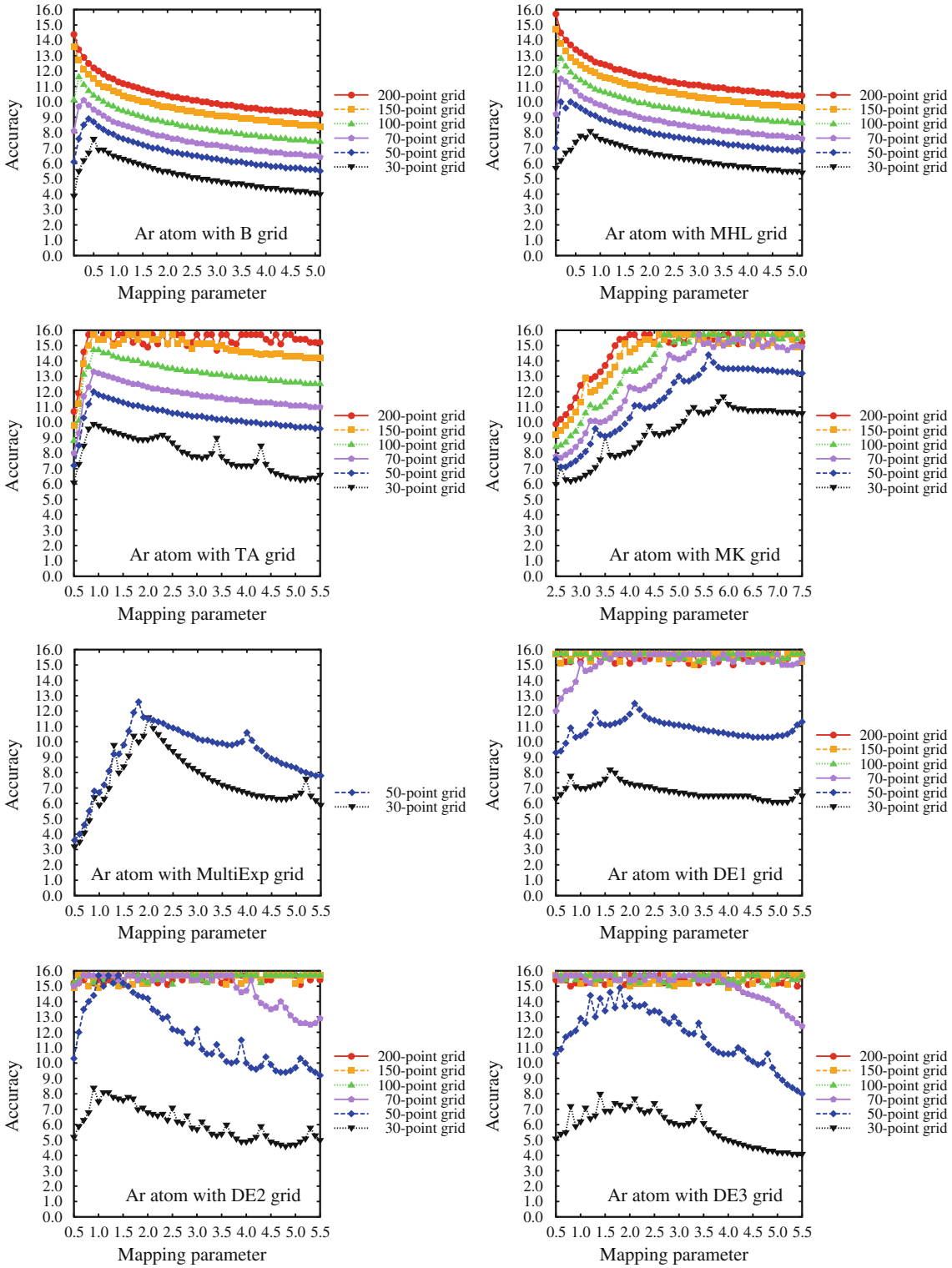

Fig. 7 Changes in Accuracy of the B, MHL, TA, MK, MultiExp, DE1, DE2, and DE3 grids for the electron-counting integral of Ar atom using STO basis functions

5.2 Properties of DE formula

An overall review article of the DE formula has been published and references therein [48]. The contents about error estimation in numerical integration, variable transformation in numerical integration, discovery of the double exponential transformation, developments of the DE formula, and DE sinc methods and further

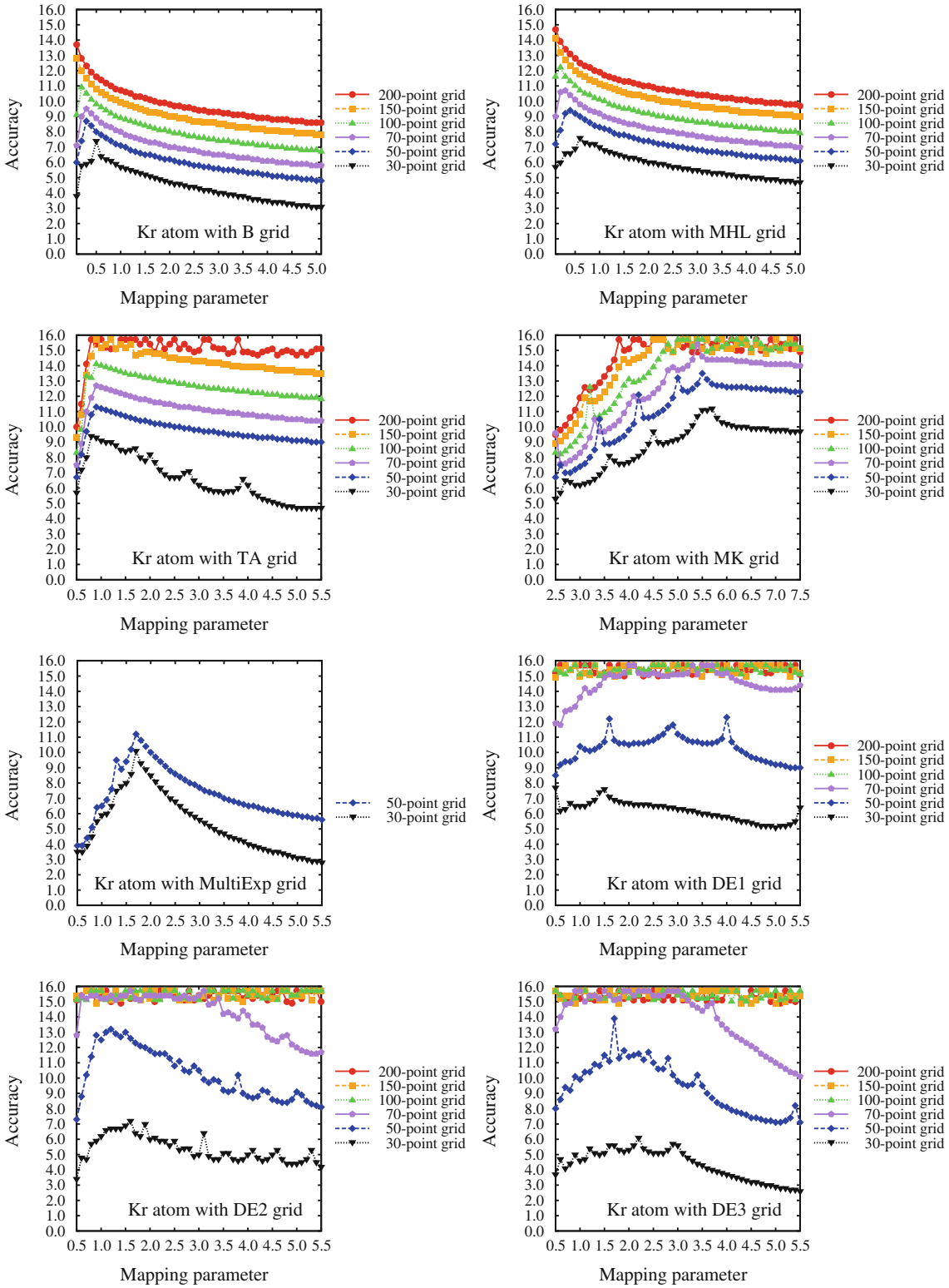

Fig. 8 Changes in Accuracy of the B, MHL, TA, MK, MultiExp, DE1, DE2, and DE3 grids for the electron-counting integral of Kr atom using STO basis functions

developments have been summarized [48]. We briefly describe fundamental properties on the DE formula in the next paragraph.

It is proved from the error estimation of typical quadrature formulas that the trapezoidal formula with an equal mesh size is optimal for numerical integration of an

Table 3 Grid ranking of the B, MHL, TA, MK, MultiExp, DE1, DE2, and DE3 grids with $n^r = 30$, 40, and 50 for the electron-counting integrals of He, Ne, Ar, and Kr atoms using GTO basis functions[a]

Atom	n^r	Grid ranking
He	30	B, MHL (5) < DE2, DE1 (7) < DE3 (8) < MK (9) < TA (10) < MultiExp (12)
	40	B (7) < DE1 (8) < MHL, DE2 (9) < DE3 (12) < TA, MK (13) < MultiExp (14)
	50	B, MHL (9) < DE1 (10) < MultiExp, DE2 (13) < DE3 (14) < TA (15) < MK (16)
Ne	30	B, MHL (4) < DE3 (5) < DE1, DE2, MultiExp (6) < TA, MK (7)
	40	MHL, B (6) < DE2, DE3 (7) < DE1, MultiExp (8) < TA, MK (9)
	50	B (7) < MHL (8) < DE3, TA, DE1 (9) < MultiExp, DE2 (10) < MK (11)
Ar	30	DE2, DE3 (4) < MHL, B, MultiExp, DE1 (5) < TA (7) < MK (8)
	40	B, MHL (5) < DE1, DE3 (6) < MultiExp, DE2 (7) < MK, TA (8)
	50	B (6) < MHL, MultiExp (7) < TA, DE2 (8) < DE3, MK (9) < DE1 (10)
Kr	30	DE3 (3) < DE2 (4) < B, MHL, TA, DE1 (5) < MultiExp, MK (6)
	40	DE3 (4) < MultiExp, MHL, DE2, DE1, B (6) < TA, MK (7)
	50	MultiExp, DE3 (6) < DE2, MHL (7) < DE1 (8) < B, TA, MK (9)

[a] Values in parentheses are order of Accuracy

Table 4 Grid ranking of the B, MHL, TA, MK, MultiExp, DE1, DE2, and DE3 grids with $n^r = 30$, 40, and 50 for the electron-counting integrals of He, Ne, Ar, and Kr atoms using STO basis functions[a]

Atom	n^r	Grid ranking
He	30	B (7) < MHL (8) < DE1 (9) < TA, MultiExp (12) < MK (14) < DE3 (15) < DE2 (16)
	40	B (8) < MHL (10) < DE1 (12) < TA (13) < MultiExp (14) < MK, DE2, DE3 (15)
	50	B (10) < MHL (12) < MultiExp (13) < TA, DE1 (14) < DE3, DE2, MK (15)
Ne	30	B (6) < DE1 (8) < MHL (9) < DE3 (10) < TA, DE2 (11) < MK, MultiExp (12)
	40	B, MHL (8) < TA, MultiExp (12) < DE1 (13) < DE3 (14) < MK (15) < DE2 (16)
	50	B (9) < MHL (10) < MultiExp (12) < TA (13) < DE1 (14) < MK (15) < DE2, DE3 (16)
Ar	30	B, MHL (6) < DE3 (7) < DE1, DE2 (8) < TA (10) < MK (11) < MultiExp (12)
	40	B, MHL (7) < DE1 (10) < DE3, TA, MultiExp (11) < DE2, MK (13)
	50	B (8) < MHL (10) < DE1 (11) < MultiExp, TA (12) < MK (14) < DE3 (15) < DE2 (16)
Kr	30	DE3, B, MHL, DE1, DE2 (6) < TA (9) < MultiExp (10) < MK (11)
	40	B, MHL (7) < DE1, DE3 (9) < TA, MultiExp, DE2 (11) < MK (14)
	50	B (7) < MHL (8) < MultiExp, TA (11) < DE1, DE2 (12) < MK (13) < DE3 (14)

[a] Values in parentheses are order of Accuracy

Table 5 The smallest number of grid points with Accuracy > 15 for the electron-counting integrals of He, Ne, Ar, and Kr atoms by the TA, MK, DE1, DE2, and DE3 grids

Basis function	Atom	TA	MK	DE1	DE2	DE3
GTO	He	60	50	80	70	60
	Ne	90	80	90	80	100
	Ar	130	110	100	100	130
	Kr	150	120	100	110	140
STO	He	80	40	60	30	30
	Ne	90	60	60	40	50
	Ar	110	80	70	50	60
	Kr	130	90	70	60	60

analytic function over $(-\infty, \infty)$. A variable transformation that maps the original interval of integration on $(-\infty, \infty)$ is introduced to take advantage of this optimality. The discretization and truncation errors of such formula are discussed in relation to the decay behavior for the transformed integrand. It is shown that

Table 6 Accuracy of the TA, MK, DE2, and AQR grids for the electron-counting integrals of He, Ne, and Ar atoms using GTO basis functions

Atom	n^r	TA	MK	DE2	AQR[a]
He	30	9.7	9.3	7.1	9.8
	33				11.5
	37				12.4
	39				13.8
	40	12.8	13.1	9.1	
Ne	30	6.9	7.0	5.9	
	34				7.4
	39				8.8
	40	9.1	9.3	7.0	
	45				9.8
	50	9.2	10.7	9.9	
	52				10.7
	55				11.7
	57				12.8
	60	12.0	13.2	10.6	
	69				14.1
	70	12.3	14.0	13.6	
Ar	30	6.5	7.6	4.2	
	31				6.0
	40	8.3	8.1	7.2	
	41				7.0
	50	8.4	9.1	8.4	7.8
	58				9.8
	60	9.6	9.9	10.6	
	63				10.0
	69				10.8
	70	9.9	10.4	11.5	
	79				12.4
	80	12.0	12.4	13.0	
	85				13.4
	89				13.7
	90	11.8	12.5	14.4	

[a] Accuracies of AQR grid are taken from Ref. [12]

the overall error becomes large in both cases where the decay of the transformed integrand is too fast and too slow. Consequently, the transformation function should be an optimal decay between these two cases. A sequence of transformations which gives a different decay is examined analytically and compared numerically. It is confirmed that the double exponential decay is optimal. The error of the DE formula is expressed as $O(\exp(-cN/\log N)$, where N is the number of sampling points (c is a positive constant). Therefore, the DE grid converges fast as N becomes large. It is concluded that the trapezoidal formula combined with the DE transformation is optimal in the sense that there exists no quadrature formula obtained by variable transformation whose error decays faster than the DE formula for large N. The DE formula is successfully used in the fields of molecular physics, fluid dynamics, statistics, civil engineering, financial engineering, the boundary element method, and so on. Examples for applications of the DE integration in these fields are found in Ref. [48].

In the previous subsection, we demonstrated that the sweet spot of the mapping parameter is relatively wide for the DE formula on the basis of the electron-counting integrals for noble gas atoms. It is, thus, expected that the DE formula is useful for molecular integrals without fine tuning of the DE grids for each atom. The results of the electron-counting integrals for diatomic molecules are given in the following subsection. Further study of multi-center integration with the DE grids is now in progress for other molecular systems including polyatomic molecules larger than diatomic molecules. We will report the results elsewhere. The DE formula is also applicable to the AQR method instead of the Gauss–Legendre and Gauss–Laguerre formulas in order to carry out the numerical integration over each of subintervals since the required DE transformation has been proposed already [26–30].

5.3 Electron-counting integral for diatomic molecule

We performed numerical integration of the electron-counting integrals for LiH, NaH, KH, Li_2, Na_2, K_2, HF, HCl, HBr, F_2, Cl_2, Br_2, LiF, NaCl, KBr, $[ScH]^+$, $[MnH]^+$, and $[CuH]^+$ molecules as demonstrative applications of the DE formula to multi-center integrals. The ionically bonded (LiH, NaH, KH, LiF, NaCl, and KBr) and covalently bonded (Li_2, Na_2, K_2, HF, HCl, HBr, F_2, Cl_2, Br_2) diatomic molecules including alkali metals and halogens up to third-row elements were tested to examine the effects of different atomic environment in molecules on the performance of each radial grid. The examinations of alkali metal hydrides and alkali metal hologenides using the DE formula are valuable since it has been described in Ref. [10] that all current quadrature schemes give very poor results with fine grids for LiH and LiF molecules. The transition metal hydride cations containing Sc, Mn, and Cu atoms were also examined to investigate whether different number of 3d electrons affects the performance of each radial grid or not. In this subsection, we compare the results obtained from the TA, MK, DE1, DE2, and DE3 calculations which give accurate numerical integration of the electron-counting integrals for atomic system.

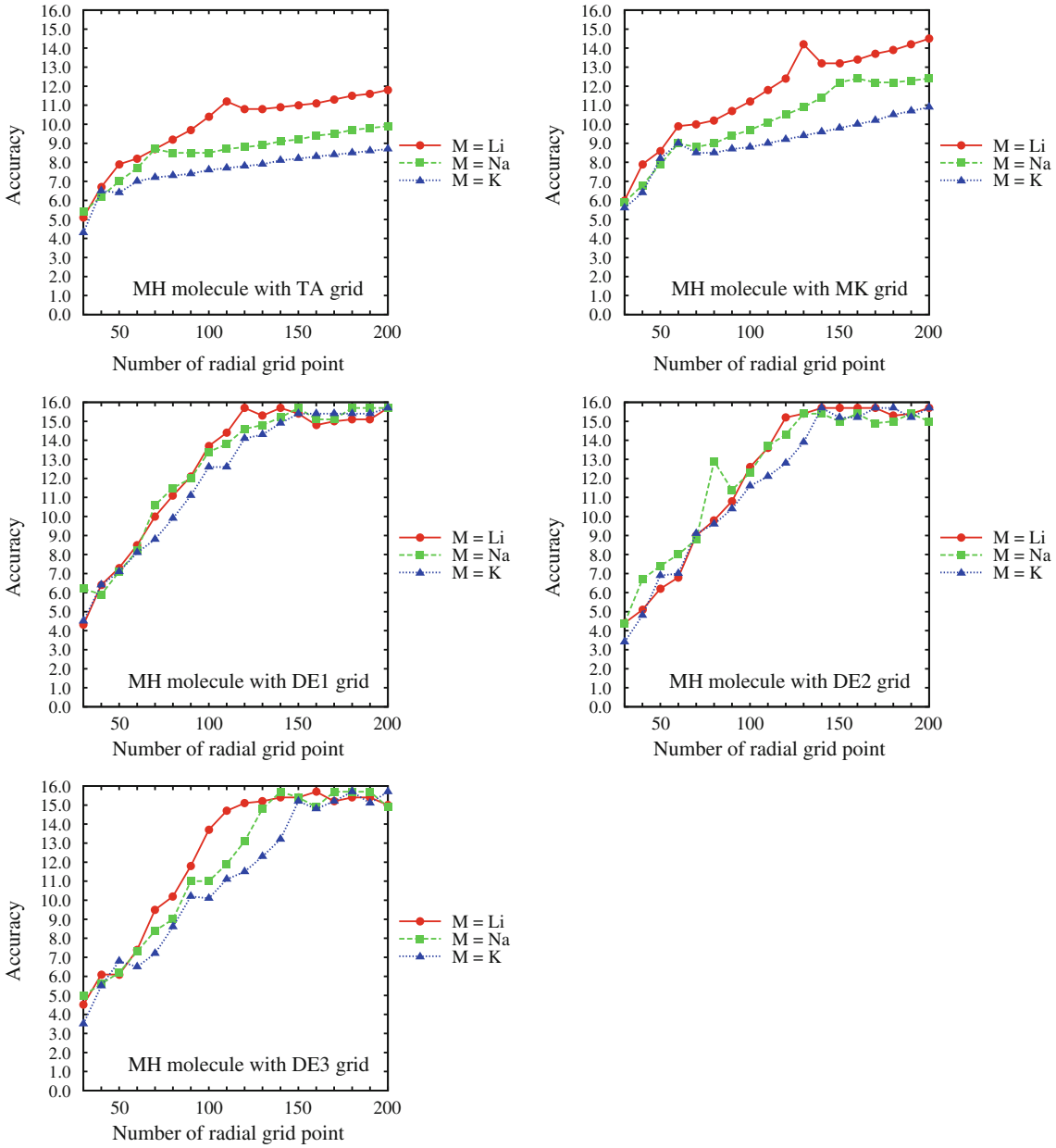

Fig. 9 Convergence behavior of Accuracy by the TA, MK, DE1, DE2, and DE3 radial grids combined with Lebedev angular grid ($n^{\Omega} = 1202$) for the electron-counting integrals of LiH, NaH, and KH molecules

Figures 9, 10, 11, 12, 13, and 14 show the convergence behavior of each quadrature approximation for the numerical integration of the electron density as Fig. 9 for MH (M = Li, Na, K) molecules, Fig. 10 for M_2 (M = Li, Na, K) molecules, Fig. 11 for HX (X = F, Cl, Br) molecules, Fig. 12 for X_2 (X = F, Cl, Br) molecules, Fig. 13 for MX (MX = LiF, NaCl, KBr) molecules, and Fig. 14 for $[MH]^+$ (M = Sc, Mn, Cu) molecules. Full list of Accuracy using TA, MK, and DE radial grids is also given in Online Resources 3, 4, and 5 as Tables S3, S4, and S5 for MH and M_2, HX and X_2, and MX and $[MH]^+$ molecules, respectively.

It is clearly found from Figs. 9, 10, 11, 12, 13, and 14 that the TA and MK radial grids give significantly poor convergence of Accuracy for the MH and MX molecules compared with the M_2, HX, and X_2 molecules as mentioned in Ref. [10]. The TA and MK radial grids also show slow convergence for the $[MH]^+$ molecules. It is obvious that the convergence behavior of the DE radial grids is better than the TA and MK radial grids for these

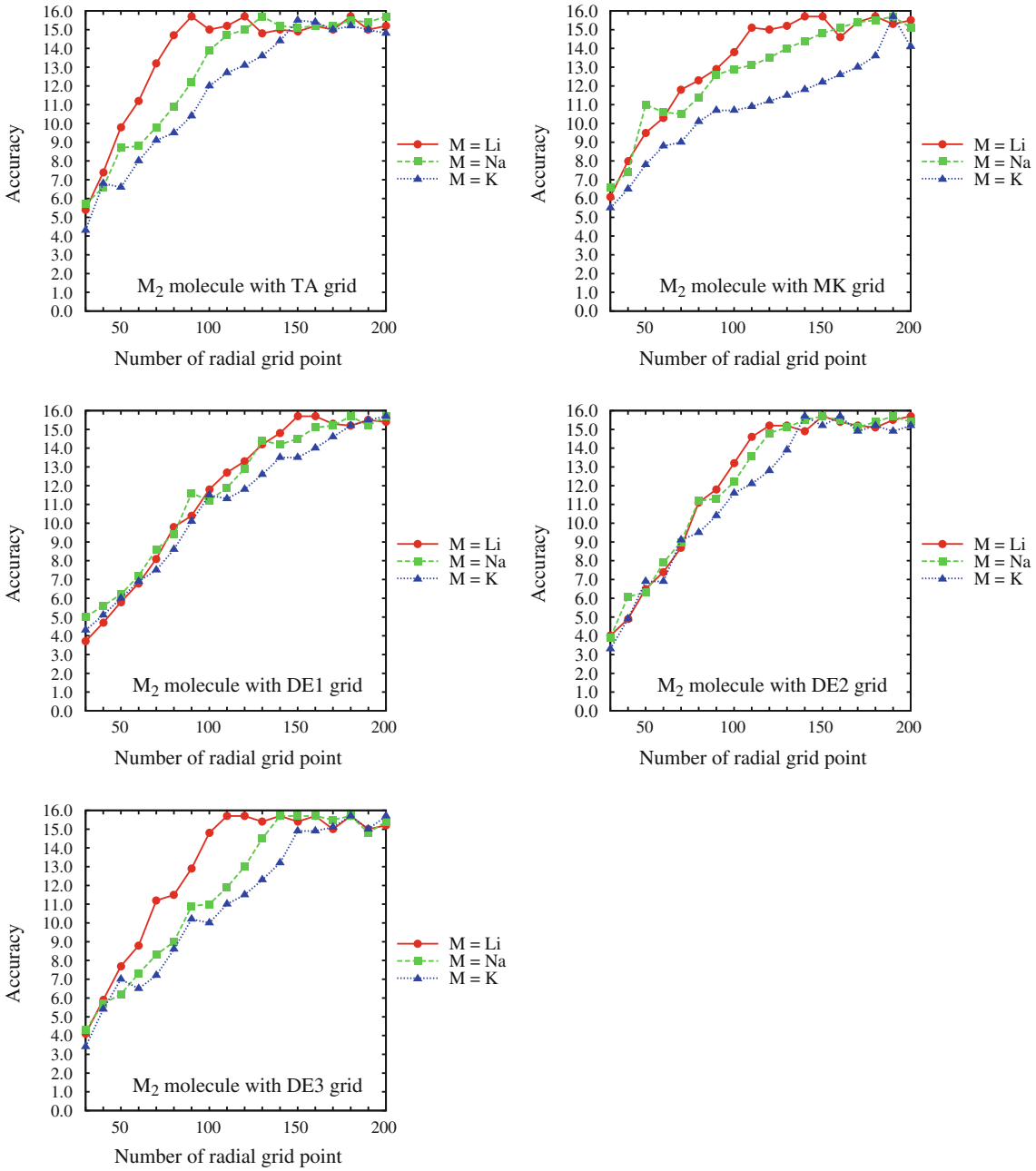

Fig. 10 Convergence behavior of Accuracy by the TA, MK, DE1, DE2, and DE3 radial grids combined with Lebedev angular grid ($n^{\Omega} = 1202$) for the electron-counting integrals of Li_2, Na_2, and K_2 molecules

molecules. Although all the radial grids need more sampling points to converge by exchanging the atom constructing diatomic molecules from light to heavy element, this trend of slow convergence is not remarkable for the DE1, DE2, and DE3 quadrature schemes than for the TA and MK quadrature schemes as seen in Figs. 10 (M_2), 11 (HX), and 12 (X_2). The performance of the MK integration becomes especially poor for the molecules with third-row element in contrast to the molecules with first- or second-row element (Figs. 10, 11, 12). Moreover, Accuracy of the TA and MK formulas for transition metal hydride cations largely depends on atomic species as Cu > Mn ≫ Sc, whereas the DE1, DE2, and DE3 formulas show similar behavior of Accuracy for these transition metals, respectively (Fig. 14).

We extract the smallest number of radial grid points required to achieve Accuracy > 15 from Tables S3–S5 (Online Resources 3–5) in Table 7. The integrated values

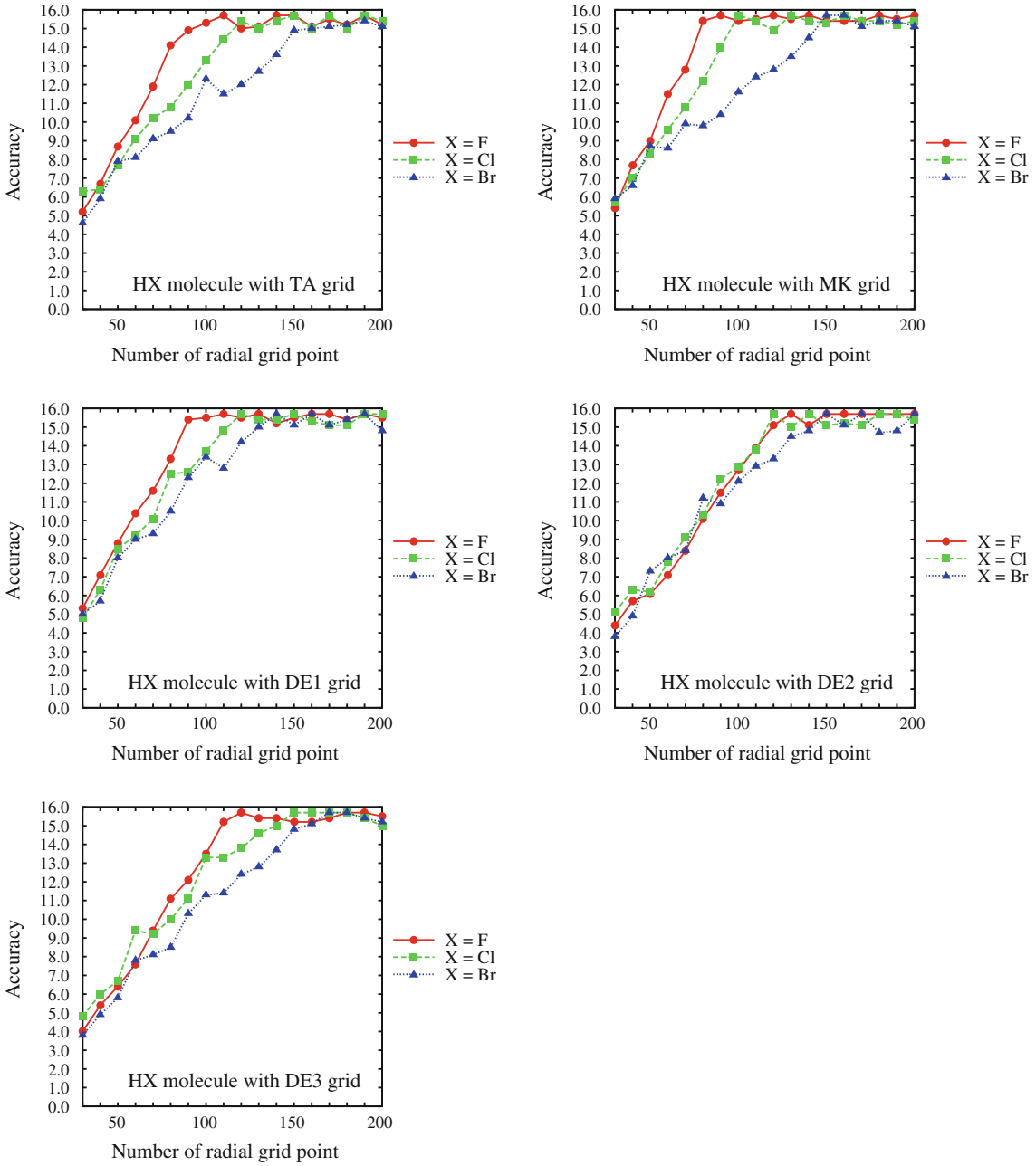

Fig. 11 Convergence behavior of Accuracy by the TA, MK, DE1, DE2, and DE3 radial grids combined with Lebedev angular grid ($n^{\Omega} = 1202$) for the electron-counting integrals of HF, HCl, and HBr molecules

of the TA and MK results for alkali metal hydrides, alkali metal halogenides, and transition metal hydride cations do not converge to high accuracy (Accuracy > 15) except for the $[MnH]^+$ and $[CuH]^+$ molecules with the MK scheme even if the 200-point radial grid is used. On the other hand, Accuracy of the DE radial grids converges to the exact value for all the molecules within the numbers of radial grid points examined in this study. It is confirmed form a comparison between the TA and MK radial grids that the TA grid is efficient for the Li_2, Na_2, K_2, and KBr molecules while the MK grid is efficient for the other molecules, indicating the performance of radial grids depends on molecular species. The required number of sampling points for the M_2, HX, and X_2 molecules to obtain the results with high accuracy (Accuracy > 15) ranges from 90 to 170 for the TA grid and from 80 to 190 for the MK grid. The required number for all the molecules is 90–180, 110–150, and 110–180 for the DE1, DE2, and DE3 grids,

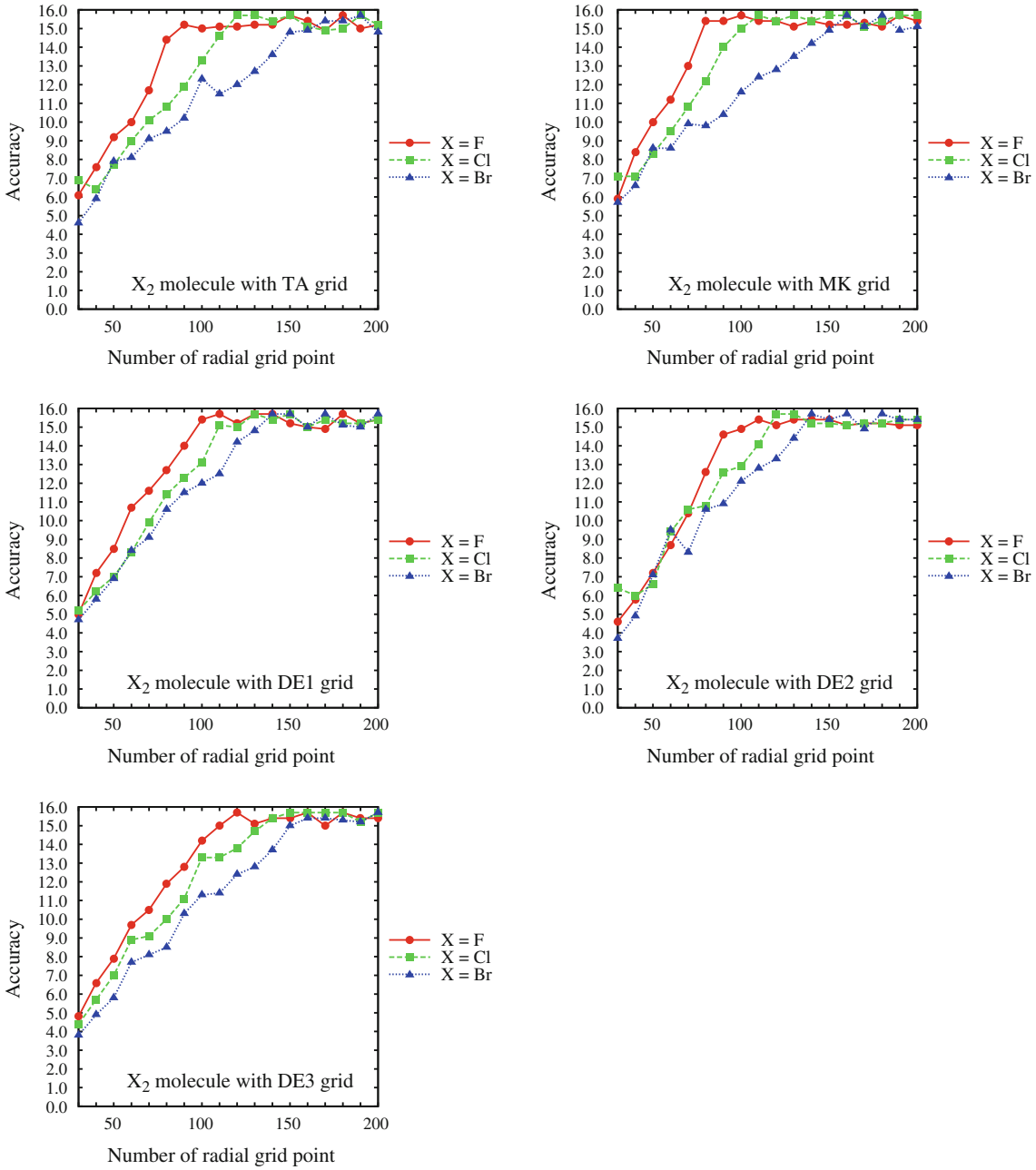

Fig. 12 Convergence behavior of Accuracy by the TA, MK, DE1, DE2, and DE3 radial grids combined with Lebedev angular grid ($n^{\Omega} = 1202$) for the electron-counting integrals of F_2, Cl_2, and Br_2 molecules

respectively. The molecular dependence of the DE2 grid is relatively small compared with the other grids. The DE2 grid also converges to the exact value faster than the TA or MK grid as follows: faster than the MK grid for Na_2 molecule, faster than the TA and MK grids for K_2 molecules, faster than the TA grid for HBr molecule, faster than the TA and MK grids for Br_2 molecule, demonstrating that the DE2 formula improves the convergence of Accuracy for the molecules with heavy element. The performance of the DE1 grid is similar to or better than the DE2 grid except for the Li_2, Na_2, and K_2 molecules. The convergence of the DE3 grid becomes slow with the replacement of light atom by heavy atom from first- to third-row element in comparison with the DE1 and DE2 grids.

The average value of Accuracy over all the diatomic molecules is summarized in Table 8 for each radial grid together with the standard deviation of Accuracy. The TA and MK quadrature estimations are superior to the DE

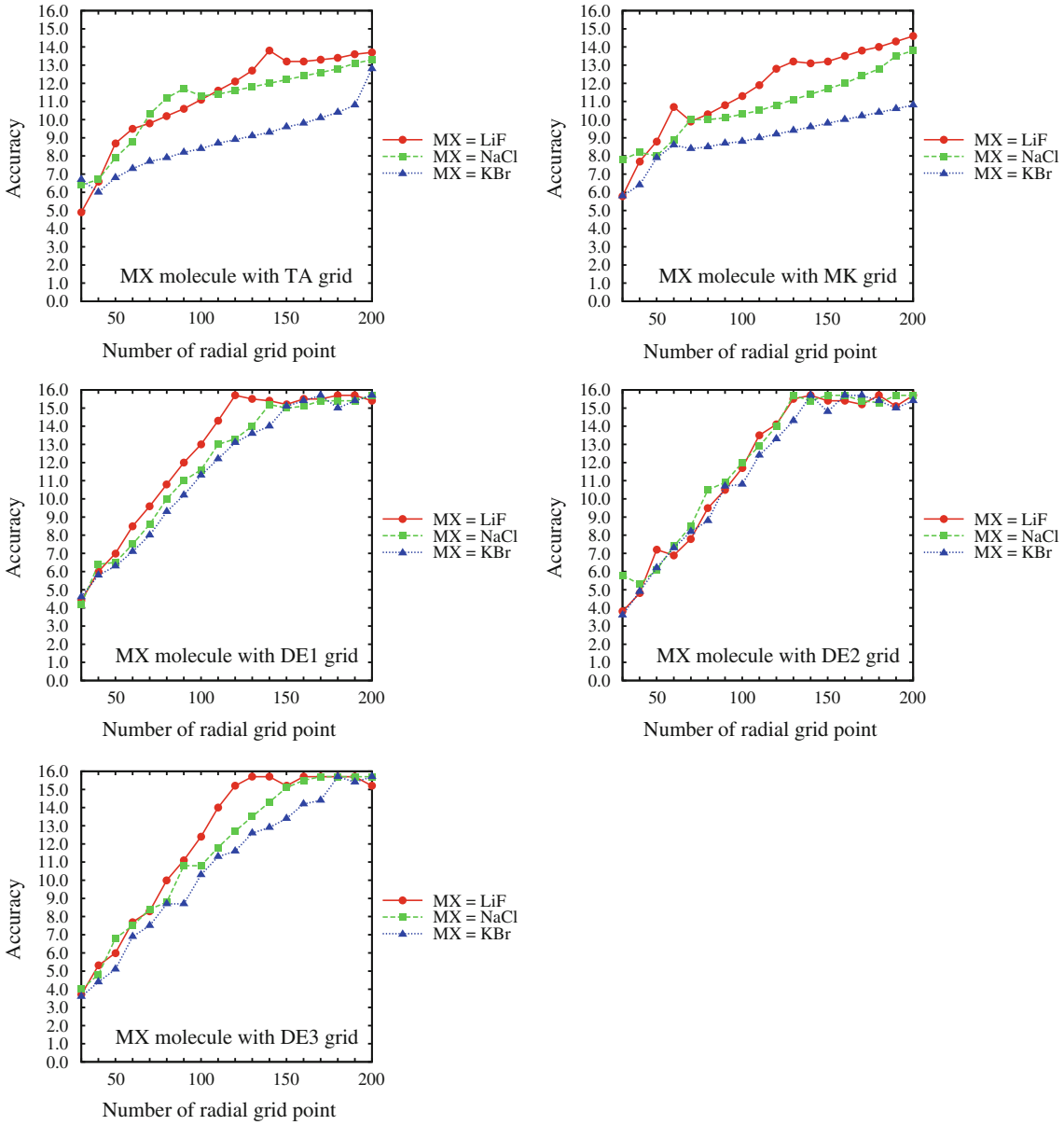

Fig. 13 Convergence behavior of Accuracy by the TA, MK, DE1, DE2, and DE3 radial grids combined with Lebedev angular grid ($n^{\Omega} = 1202$) for the electron-counting integrals of LiF, NaCl, and KBr molecules

quadrature estimations for radial grids smaller than the 100-point grid, while the DE integration schemes are superior to the TA and MK integration schemes for radial grids larger than the 100-point grid. Moreover, the dispersion of Accuracy concerning the radial grids with 70 or more grid points is smaller in the DE radial grids than in the TA and MK radial grids. Especially for the 150- to 200-point radial grids, the standard deviations of Accuracy for the DE grids are very small, indicating that the behavior of the DE grids is stable for all the molecules in contrast to the TA and MK grids.

6 Concluding remarks

In this study, we investigated the performance of the DE formula on the numerical integration of the radial electron distribution function for atomic and diatomic molecular systems represented by the GTO or STO basis functions. Three-type DE transformations were introduced into the radial quadrature scheme to generate new radial grids. The accuracy and convergence of the DE grids were compared with those of the B, MHL, TA, MK, and MultiExp grids for the electron-counting integrals of He, Ne, Ar, and Kr atoms

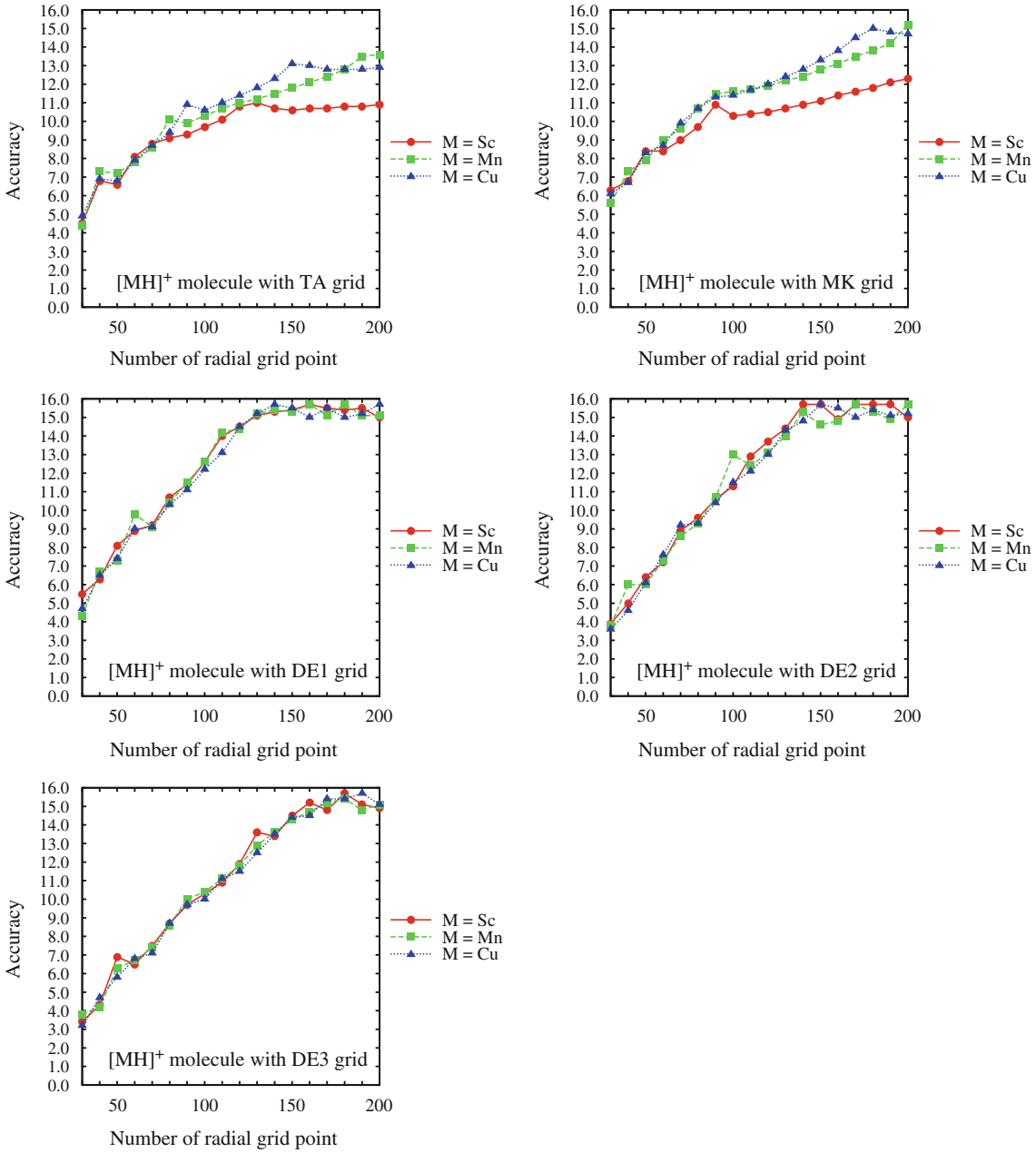

Fig. 14 Convergence behavior of Accuracy by the TA, MK, DE1, DE2, and DE3 radial grids combined with Lebedev angular grid ($n^{\Omega} = 1202$) for the electron-counting integrals of $[ScH]^+$, $[MnH]^+$, and $[CuH]^+$ molecules

and of LiH, NaH, KH, Li_2, Na_2, K_2, HF, HCl, HBr, F_2, Cl_2, Br_2, LiF, NaCl, KBr, $[ScH]^+$, $[MnH]^+$, and $[CuH]^+$ molecules.

The results reveal that fast convergence of the integrated values to the exact value is achieved by applying the DE formula. The DE grids show similar or higher accuracies than the other grids particularly for the Kr atom. Furthermore, the DE-Lebedev quadrature schemes give stable performance for all the diatomic molecules compared with the TA- and MK-Lebedev quadrature schemes. Especially, the DE integrations converge fast to high accuracy even for alkali metal hydrides, alkali metal halogenides, transition metal hydride cations, or diatomic molecules with heavy element in contrast to poor convergence of the TA and MK integrations. It is suggested that the DE transformations have potential ability to improve the reliability and efficiency of the numerical integration for energy functionals if combined with an

Table 7 The smallest number of radial grid points with Accuracy > 15 for the electron-counting integrals of LiH, NaH, KH, Li_2, Na_2, K_2, HF, HCl, HBr, F_2, Cl_2, Br_2, LiF, NaCl, KBr, $[ScH]^+$, $[MnH]^+$, and $[CuH]^+$ molecules by the TA, MK, DE1, DE2, and DE3 radial grids combined with Lebedev angular grid ($n^\Omega = 1202$)

Molecule	TA	MK	DE1	DE2	DE3
LiH	NC[a] (11.8)[b]	NC[a] (14.5)[b]	120	120	120
NaH	NC[a] (9.9)[b]	NC[a] (12.4)[b]	140	130	140
KH	NC[a] (8.7)[b]	NC[a] (10.9)[b]	150	140	150
Li_2	90	110	150	120	110
Na_2	120	160	160	130	140
K_2	150	190	180	140	170
HF	100	80	90	120	110
HCl	120	100	120	120	140
HBr	160	150	130	150	160
F_2	90	80	100	110	110
Cl_2	120	100	110	120	140
Br_2	170	160	140	140	150
LiF	NC[a] (13.7)[b]	NC[a] (14.6)[b]	120	130	120
NaCl	NC[a] (13.3)[b]	NC[a] (13.8)[b]	140	130	150
KBr	NC[a] (12.8)[b]	NC[a] (10.8)[b]	150	140	180
$[ScH]^+$	NC[a] (10.9)[b]	NC[a] (12.3)[b]	130	140	160
$[MnH]^+$	NC[a] (13.6)[b]	200	130	140	170
$[CuH]^+$	NC[a] (12.9)[b]	180	130	150	170

[a] Accuracy does not converge to 15 or higher at $n^r = 200$

[b] Values in parentheses are Accuracy at $n^r = 200$

Table 8 Average Accuracy of the TA, MK, DE1, DE2, and DE3 radial grids combined with Lebedev angular grid ($n^\Omega = 1202$) for the electron-counting integrals of LiH, NaH, KH, Li_2, Na_2, K_2, HF, HCl, HBr, F_2, Cl_2, Br_2, LiF, NaCl, KBr, $[ScH]^+$, $[MnH]^+$, and $[CuH]^+$ molecules[a]

n^r	TA	MK	DE1	DE2	DE3
30	5.3 (0.8)	6.0 (0.6)	4.8 (0.6)	4.2 (0.8)	4.0 (0.5)
40	6.6 (0.5)	7.2 (0.6)	6.1 (0.6)	5.4 (0.6)	5.3 (0.7)
50	7.7 (0.9)	8.6 (0.8)	7.2 (0.8)	6.6 (0.5)	6.5 (0.7)
60	8.6 (1.1)	9.5 (0.9)	8.5 (1.1)	7.7 (0.8)	7.6 (1.0)
70	9.6 (1.5)	10.1 (1.3)	9.4 (1.1)	8.9 (0.7)	8.5 (1.1)
80	10.4 (2.0)	10.9 (1.9)	10.7 (1.2)	10.4 (1.1)	9.5 (1.1)
90	11.1 (2.3)	11.6 (2.1)	11.8 (1.3)	11.3 (1.0)	10.8 (1.1)
100	11.7 (2.3)	12.0 (2.2)	12.8 (1.2)	12.3 (0.9)	11.8 (1.6)
110	12.0 (2.4)	12.3 (2.2)	13.6 (1.3)	13.3 (0.9)	12.6 (1.6)
120	12.3 (2.4)	12.6 (2.0)	14.3 (1.1)	14.1 (1.0)	13.2 (1.6)
130	12.5 (2.4)	13.0 (2.0)	14.8 (0.8)	14.9 (0.6)	13.9 (1.2)
140	12.8 (2.4)	13.2 (2.0)	15.1 (0.6)	15.4 (0.3)	14.5 (1.0)
150	13.2 (2.5)	13.4 (1.9)	15.3 (0.5)	15.4 (0.3)	15.0 (0.6)
160	13.1 (2.3)	13.6 (1.9)	15.2 (0.4)	15.4 (0.3)	15.2 (0.5)
170	13.2 (2.3)	13.7 (1.7)	15.3 (0.3)	15.3 (0.3)	15.3 (0.4)
180	13.4 (2.3)	14.0 (1.7)	15.4 (0.2)	15.4 (0.3)	15.6 (0.1)
190	13.5 (2.2)	14.2 (1.6)	15.4 (0.2)	15.3 (0.3)	15.3 (0.3)
200	13.6 (2.0)	14.2 (1.5)	15.5 (0.3)	15.5 (0.3)	15.3 (0.3)

[a] Values in parentheses are standard deviation of Accuracy

accurate angular grid. In addition, it may be possible to further improve the DE radial grids by optimizing the mapping parameter for each atom.

References

1. Becke AD (1988) J Chem Phys 88:2547–2553
2. Lebedev VI (1975) Comp Math and Math Phys 15:44–51
3. Lebedev VI (1976) Comp Math Math Phys 16:10–24
4. Lebedev VI (1977) Sib Math J 18:99–107
5. Lebedev VI, Skorokhodov AL (1992) Russ Acad Sci Dokl Math 45:587–592
6. Lebedev VI (1995) Russ Acad Sci Dokl Math 50:283–286
7. Lebedev VI, Laikov DN (1999) Dokl Math 59:477–481
8. Murray CW, Handy NC, Laming GJ (1993) Mol Phys 78:997–1014
9. Treutler O, Ahlrichs R (1995) J Chem Phys 102:346–354
10. Mura ME, Knowles PJ (1996) J Chem Phys 104:9848–9858
11. Gill PMW, Chien S-H (2003) J Comput Chem 24:732–740
12. Kakhiani K, Tsereteli K, Tsereteli P (2009) Comput Phys Comm 180:256–268
13. Pérez-Jordá JM, Becke AD, San-Fabián E (1994) J Chem Phys 100:6520–6534
14. Krack M, Köster AM (1998) J Chem Phys 108:3226–3234
15. Lin Z, Jaffe JE, Hess AC (1999) J Phys Chem A 103:2117–2127
16. Ishikawa H, Yamamoto K, Fujima K, Iwasawa M (1999) Int J Quantum Chem 72:509–523
17. Lindh R, Malmqvist P-Å, Gagliardi L (2001) Theor Chem Acc 106:178–187
18. Köster AM, Flores-Moreno R, Reveles JU (2004) J Chem Phys 121:681–690
19. Weber V, Daul C, Baltensperger R (2004) Comput Phys Comm 163:133–142
20. El-Sherbiny A, Poirier RA (2004) J Comput Chem 25:1378–1384
21. Gill PMW, Johnson BG, Pople JA (1993) Chem Phys Lett 209:506–512
22. Chien S-H, Gill PMW (2006) J Comput Chem 27:730–739
23. Martin JML, Bauschlicher CW Jr, Ricca A (2001) Comput Phys Comm 133:189–201
24. Johnson ER, Wolkow RA, DiLabio GA (2004) Chem Phys Lett 394:334–338
25. Papas BN, Schaefer HF III (2006) J Mol Struct THEOCHEM 768:175–181
26. Takahashi H, Mori M (1974) Publ RIMS Kyoto Univ 9:721–741. Journal@rchive, Japan Science and Technology Agency (JST). http://www.journalarchive.jst.go.jp/english/jnltop_en.php?cdjournal=kyotoms1969. Accessed 14 Feb 2011
27. Mori M (1985) J Comput Appl Math 12 & 13:119–130
28. Mori M, Sugihara M (2001) J Comput Appl Math 127:287–296
29. Muhammad M, Mori M (2003) J Comput Appl Math 161:431–448
30. Tanaka K, Sugihara M, Murota K, Mori M (2009) Numer Math 111:631–655

31. Roots and Weights for MultiExp Quadrature, Quantum Chemistry at ANU. http://www.rsc.anu.edu.au/~pgill/multiexp.php. Accessed 14 Feb 2011
32. Krishnan R, Binkley JS, Seeger R, Pople JA (1980) J Chem Phys 72:650–654
33. McLean AD, Chandler GS (1980) J Chem Phys 72:5639–5648
34. Curtiss LA, McGrath MP, Blandeau J-P, Davis NE, Binning RC, Radom L (1995) J Chem Phys 103:6104–6113
35. Frisch MJ, Trucks GW, Schlegel HB, Scuseria GE, Robb MA, Cheeseman JR, Montgomery JA Jr, Vreven T, Kudin KN, Burant JC, Millam JM, Iyengar SS, Tomasi J, Barone V, Mennucci B, Cossi M, Scalmani G, Rega N, Petersson GA, Nakatsuji H, Hada M, Ehara M, Toyota K, Fukuda R, Hasegawa J, Ishida M, Nakajima T, Honda Y, Kitao O, Nakai H, Klene M, Li X, Knox JE, Hratchian HP, Cross JB, Adamo C, Jaramillo J, Gomperts R, Stratmann RE, Yazyev O, Austin AJ, Cammi R, Pomelli C, Ochterski JW, Ayala PY, Morokuma K, Voth GA, Salvador P, Dannenberg JJ, Zakrzewski VG, Dapprich S, Daniels AD, Strain MC, Farkas O, Malick DK, Rabuck AD, Raghavachari K, Foresman JB, Ortiz JV, Cui Q, Baboul AG, Clifford S, Cioslowski J, Stefanov BB, Liu G, Liashenko A, Piskorz P, Komaromi I, Martin RL, Fox DJ, Keith T, Al-Laham MA, Peng CY, Nanayakkara A, Challacombe M, Gill PMW, Johnson B, Chen W, Wong MW, Gonzalez C, Pople JA (2003) Gaussian 03, revision B.05. Gaussian, Inc., Pittsburgh
36. Bunge CF, Barrientos JA, Bunge AV (1993) At Data Nucl Data Tables 53:113–162
37. Becke AD (1993) J Chem Phys 98:5648–5652
38. Lee C, Yang W, Parr RG (1988) Phys Rev B 37:785–789
39. Hehre WJ, Ditchfield R, Pople JA (1972) J Chem Phys 56:2257–2261
40. Hariharan PC, Pople JA (1973) Theor Chim Acta 28:213–222
41. Dill JD, Pople JA (1975) J Chem Phys 62:2921–2923
42. Francl MM, Petro WJ, Hehre WJ, Binkley JS, Gordon MS, DeFrees DJ, Pople JA (1982) J Chem Phys 77:3654–3665
43. Binning RC Jr, Curtiss LA (1990) J Comput Chem 11:1206–1216
44. Blaudeau J-P, McGrath MP, Curtiss LA, Radom L (1997) J Chem Phys 107:5016–5021
45. Rassolov VA, Pople JA, Ratner MA, Windus TL (1998) J Chem Phys 109:1223–1229
46. Rassolov VA, Ratner MA, Pople JA, Redfern PC, Curtiss LA (2001) J Comput Chem 22:976–984
47. Schäfer A, Horn H, Ahlrichs R (1992) J Chem Phys 97:2571–2577
48. Mori M (2005) Publ RIMS Kyoto Univ 41:897–935. Publications of the Research Institute for Mathematical Sciences, Research Institute for Mathematical Sciences, Kyoto University. http://www.kurims.kyoto-u.ac.jp/~prims/list.html. Accessed 14 Feb 2011